Hydrodynamic Impacts of Commercial Jet-Boating on the Chilkat River, Alaska

D.F. Hill[1], M.M. Beachler, P.A. Johnson
Department of Civil & Environmental Engineering
The Pennsylvania State University
University Park, PA 16802

October 2002

[1]Contact: 814.863.7305, dfhill@engr.psu.edu

Contents

List of Figures

List of Tables

Conversion Factors

Every effort is made in this report to use the SI (metric) system of units. Some exceptions are made in order to accommodate convention. For example, units of horsepower rather than watts are used for boat engine power. Similarly, units of miles per hour rather than meters per second are used for boat speed. The following table of conversions will assist those wishing to convert reported values in SI units to BG units.

Quantity	Multiply	by	To Obtain
Area	square meter	10.77	square foot
Area	square kilometer	0.386	square mile
Area	square kilometer	247.1	acre
Energy	joules	0.738	foot pounds
Flow Rate	cubic meters per second	35.31	cubic feet per second
Flow Rate	cubic meters per second	15,850	gallons per minute
Length	meter	3.281	foot
Length	kilometer	0.622	mile
Mass	kilograms	0.685	slugs
Mass	kilograms	2.21	pounds mass
Power	watts	0.00134	horsepower
Power	watts	0.738	foot pounds per second
Speed	meters per second	2.237	miles per hour
Stress / Pressure	Pascals	0.000145	pounds per square inch

Nomenclature

The following lists and defines the variables that are used herein. Note that, in a few cases, a single symbol is used to denote multiple quantities. Every effort is made to clarify this in the text of the report.

Symbol	Description
A	area
α	wave train half-angle
β	wave amplitude decay constant
c	wave speed
d_{50}	median grain size diameter
E	wave energy density, energy
F	force
Fr	Froude number
g	gravitational acceleration
γ	fluid specific weight
h	depth
h_f	head loss
H	wave height
k	wavenumber
L	boat length
λ	wavelength
m, b	calibration constants
μ	fluid dynamic viscosity
n	Manning parameter
ν	fluid kinematic viscosity
ω	angular frequency
P	wave power
$\mathcal{P}$	wetted perimeter
Q	discharge
R_h	hydraulic radius
ρ	fluid density
S_f	friction slope
S_0	bottom slope
T	period
τ_0	bank / bed shear stress
(u, w)	horizontal & vertical velocity components

u_b	horizontal velocity at river bed
V	depth-averaged velocity, voltage
$\overline{V}$	area-averaged velocity
V_b	boat speed
x	distance from sailing line to wave gage
z	elevation

Preface

The work described in this report was conducted for the Alaska Department of Fish and Game (ADFG), Habitat and Restoration Division.

The field work was performed during May and June of 2002 by researchers from the Department of Civil and Environmental Engineering at the Pennsylvania State University. Assistance with logistical details was provided by members of ADFG. Assistance with laboratory analysis of sediment samples was provided by Ryan Whitmore.

The authors wish to thank ADFG for providing many of the on-site resources required for this study. The authors also wish to thank River Adventures for their cooperation in carrying out this study.

Summary

Measurements of boat wake height, near-bank turbidity, and near-bed water velocity induced by boat passage were made on the upper Chilkat River, near Haines, Alaska. Measurements were made for a variety of boat sizes and for a variety of operating conditions, including boat speed, passenger loading, and distance from shore. This pilot study was conducted in response to concerns about the impacts of commercial boating tours within the Chilkat Bald Eagle Preserve.

The scope of the present study is limited to understanding the physical impacts of boating on the river. Also, estimates of physical impacts associated with streamflow are made so that the *relative* impacts of boating can be judged. The more involved question of assessing the potential biological impacts of boating is left to future work.

A total of 68 trials were performed using six different boats. In the cases of boats belonging to the Alaska Department of Fish and Game (ADFG), controlled experiments were performed. In the cases of boats belonging to the commercial concession on the river, semi-controlled experiments were performed. For example, the authors had control over the path of travel of the commercial boats, but no control over the speed or passenger loading.

Some of the key findings of this report include:

- Turbidity measurements at the banks clearly demonstrate that boat wakes are capable of dislodging sediments from the banks. Peak values of suspended sediment concentration far outweigh the ambient load of the river and are found to increase with increasing wake height.

- Boat wakes are found to increase in amplitude with increasing boat size. Measurements suggest that the wake train of the largest commercial boat studied contains roughly 10 times the energy of that of the smaller ADFG boat studied.

- While there is a well-known dependence upon boat speed (confirmed by the controlled measurements), boats navigating the upper Chilkat River tend to travel in a fairly narrow band of speed. This is largely due to the necessity of keeping the boats 'on-plane', or 'on-step'. Given the shallow water depths, these speeds ($15 - 25$ mph) correspond to high depth- and length-based Froude numbers. This is beneficial in minimizing wave heights at the banks.

- Boat wakes are found to decrease in amplitude with sailing line-to-bank distance. An equation is obtained which allows for the prediction of expected wave height at the bank as a function of boat size and sailing line distance. If a maximum allowable wave height at the bank is specified, this allows for the calculation of a minimum sailing line distance.

- Comparisons of streamflow and boat wake energy suggest that, in larger channels, boat wakes only make up 2-5% of the total energy dissipated annually against the banks. In smaller channels, the roles are reversed and the streamflow makes up only 2-5% of the annual energy dissipated.

- Comparisons of streamflow and boat wake *power* suggest that, in all channels, the *rate* of energy dissipation by boat wakes exceeds that of the streamflow.

- Comparisons of streamflow and boat wake shear stress at the banks suggest that the wakes are capable of exerting a larger shear stress than the streamflow.

In conclusion, it is the authors' belief that, despite the relatively low usage levels on the Chilkat River, the potential impacts associated with boating can not be ruled out. There is sufficient evidence for continued, longer-term monitoring of the situation. Additionally, studies that directly consider the impacts of boat-associated hydraulic disturbances on spawning and rearing fish should be considered.

Chapter 1

Introduction

1.1 Historical Overview of the Chilkat River Basin

The Chilkat River basin, consisting of the Chilkat, Klehini, Tsirku, and Kelsall Rivers, lies approximately 80 miles northwest of Juneau, Alaska, and drains into the upper Lynn Canal. A significant portion of the basin overlaps with the 49,000 acre Chilkat Bald Eagle Preserve (CBEP). The preserve was designated by the State Legislature in 1982. Prior to this, the importance of the large fall / winter gatherings of bald eagles was recognized through the designation of a 4800 acre Critical Habitat Area in 1973 and the adoption of the Haines / Skagway Land Use Plan in 1979.

As described in Alaska statute, and as reviewed by the Alaska Department of Natural Resources (ADNR, 2002), the CBEP was created to:

- Protect and perpetuate the Chilkat bald eagles and their essential habitats within the preserve,
- Protect and sustain the natural salmon spawning and rearing areas of the Chilkat River and Chilkoot River systems in perpetuity,
- Provide continued opportunities for research, study, and enjoyment of bald eagles and other wildlife,
- Maintain water quality and necessary water quality,

- Provide for the continued traditional and natural resource based lifestyle of the people living in the area, and
- Provide for other public uses consistent with the primary purpose of the Preserve.

In 1985, a plan for managing the Preserve was adopted. During the period of 2001-2002, a revision process for the plan has been underway. One of the issues of concern, and the one pertinent to the present study and report, is that the Preserve has experienced greatly increasing levels of commercial recreational use over the past 10 years. The specific commercial use of relevance to the present study is that of large-scale jet-boat tours of the upper Chilkat River, between Wells Bridge and the confluence with the Kelsall River.

Concern that operation of these large jet-boats is having an impact on salmon habitat prompted the ADFG to contact the authors and to sponsor a three-week hydraulic study of these impacts. The anticipated outcome of the study, at the time of the initial discussions, was a set of objective data on the hydraulic disturbances of these boats. These data would then be available for incorporation into management decisions regarding the revised Preserve plan.

1.2 Study Scope and Limitations

The fundamental question underlying this study and report, whether or not operation of large-scale jet-boat tours adversely impacts salmon habitat, is extremely complex. However, it can conceptually be broken down into three distinct parts. First, the physical impacts of jet-boating must be understood. These impacts include (i) the generation of wakes, which radiate from the sailing line of a boat and eventually impinge upon the banks of the river, and (ii) the modification to the flow of the river that occurs due to hull-displacement and propulsion effects. If of sufficient magnitude, both of these mechanisms have the potential to dislodge and transport sediment. If this is the case, then the operation of a boat can be said to be having a distinct impact on the river.

Second, the magnitudes of these impacts should be compared to naturally occurring processes in the river system. As an example, the annual amount of energy dissipated on the river banks by boat wakes can be compared to

that of the background flow of the river. While there are differences between these mechanisms (e.g. boat wakes impinge upon banks on an angle while currents flow tangential to the banks), this sort of calculation is helpful in an 'order of magnitude' sense.

Finally, provided that boating results in hydraulic signals that are strong enough to emerge from the background noise of the river, there is the question of whether or not that impact is of significance. In the context of the present study, this is really a biological question, seeking to answer whether or not salmon are impacted by the increased sediment loads and / or turbulence associated with boat wakes and bottom-scouring.

The present study, planned and executed with limited time and resources, is most properly viewed as a 'pilot' study. Accordingly, it can not be expected to provide a conclusive quantitative answer to the question of whether or not jet-boating on the Chilkat River is having a deleterious effect on salmon populations. Rather, it was the intent of the authors to focus attention on the first and second parts of the overall question, as discussed above. Given a solid set of data on the wakes present on the Chilkat River, these data can be interpreted in light of other, more extensive bank-erosion studies conducted elsewhere. The data can also be used in planning additional studies that more directly address the question of biological impacts.

Also, it should be stressed that erosion is not an 'instantaneous' phenomenon but, rather, a cumulative long-term process. As such, it is difficult to quantify, given a single, three-week field season, an amount of bank-recession associated with boating activity. Regardless of the management decisions that may result from the data presented here, the authors stress the need for a longer-term monitoring program to be put in place. Such a program will begin to provide data that can be used to, on an annual basis, evaluate changes in the river.

1.3 Report Outline

A brief hydrologic review of the Chilkat River Basin, adapted from Bugliosi (1985), is presented in Chapter 2, along with a brief review of previous studies on boating impacts. As much of the present report focuses on water waves, a brief discussion of wave mechanics is given in Chapter 3 for the benefit of the reader unfamiliar with the topic. Chapter 4 describes the experimental sites, facilities and instrumentation while Chapter 5 presents the experimen-

tal methodology and the obtained data. Chapter 6 provides discussion of the results and pertinent calculations and, finally, Chapter 7 provides the conclusions and a discussion of additional work that should be done.

Chapter 2

Background

This chapter provides a brief quantitative overview of some of the pertinent hydrologic characteristics of the Chilkat River basin and a detailed review of relevant literature on boating impacts in general.

2.1 Hydrologic Overview of Chilkat Basin

The Chilkat River basin (Figs. 2.1-2.4) lies in southeast Alaska, at the head of the Lynn Canal. A thorough description of the geologic and hydrologic characteristics of the basin is given by Bugliosi (1985) and will therefore only be summarized here.

The basin is approximately 2500 km^2 in horizontal extent and is characterized by braided channels in glaciated valleys. The system is largely glacially fed, with a correspondingly strong annual variation being observed in the river hydrograph.

Streamflow in the basin comes from both runoff and groundwater sources. Quantitative data on the discharges of the major streams in the Chilkat basin are quite limited and are summarized in Table 2.1. From this data, it can be estimated that the maximum and minimum flows being discharged into the Lynn Canal are 630 and 16 $m^3\ s^{-1}$ respectively.

The strong annual cycle is evident in Fig. 2.5, which details the monthly mean flows for the Chilkat and Klehini Rivers near Klukwan. The highest flows, driven by glacier melt, are observed in summer months. High flows can also occur during early autumn months, driven in part by rainfall.

During mid-winter to mid-spring, the low flows observed are sustained

Stream	Period of Record	Maximum Discharge (m^3 s^{-1})	Minimum Discharge (m^3 s^{-1})
Chilkat River near Klukwan	1981-1982	201	8.5
Klehini River near Klukwan	1982-1983	255	3.3
Tsirku River near Klukwan	1981-1983	153	4.0
Takhin River at mouth	1981-1982	20.4	–

Table 2.1: Maximum and minimum discharges for streams in the Chilkat River basin. Data adapted from Bugliosi (1985)

in part by groundwater discharges. Of particular interest is the discharge of relatively warm water at the Tsirku River alluvial fan. This water helps to maintain open stretches of the lower Chilkat River, which are directly responsible for a late-season run of salmon and, therefore, indirectly responsible for the gathering of bald eagles in the winter months. Accurate measurements of groundwater discharge are more difficult than those of streamflow, but the water budget of Bugliosi (1985) suggests that a daily average of 18.1 m^3 s^{-1} is discharged from the fan into the Chilkat River.

Finally, the order of magnitude of the suspended sediment load of the streams in the Chilkat basin can be estimated from measurements by Bugliosi (1985). Measurements of suspended sediment concentration and streamflow discharge were made on three streams during a period of high flow and a period of low flow, as summarized in Table 2.2.

	Chilkat River near Klukwan		Klehini River near Klukwan		Tsirku River above fan	
Date	8/15/81	4/6/82	8/15/81	4/6/82	8/15/81	4/6/82
Susp. Sed. Conc. (mg l^{-1})	361	16	716	1	1530	1
Discharge (m^3 s^{-1})	201.0	8.5	99.4	5.4	152.6	4.0
Sediment Load (metric tons per day)	6270	12	6148	0.5	20,173	0.3

Table 2.2: Suspended sediment concentrations, streamflow discharges, and total sediment loads. Data are representative of typical high flow and low flow conditions and are adapted from Bugliosi (1985).

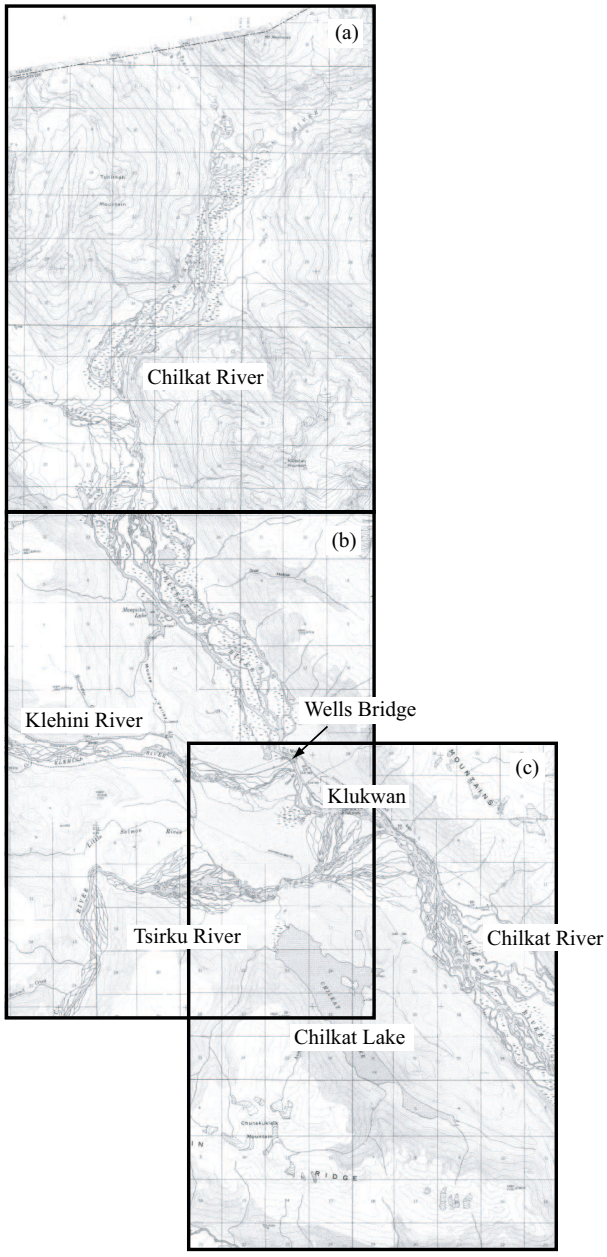

Figure 2.1: Topographic view of the Chilkat River basin. Source: USGS 7.5 minute Skagway B-3 & C-3 quadrangles.

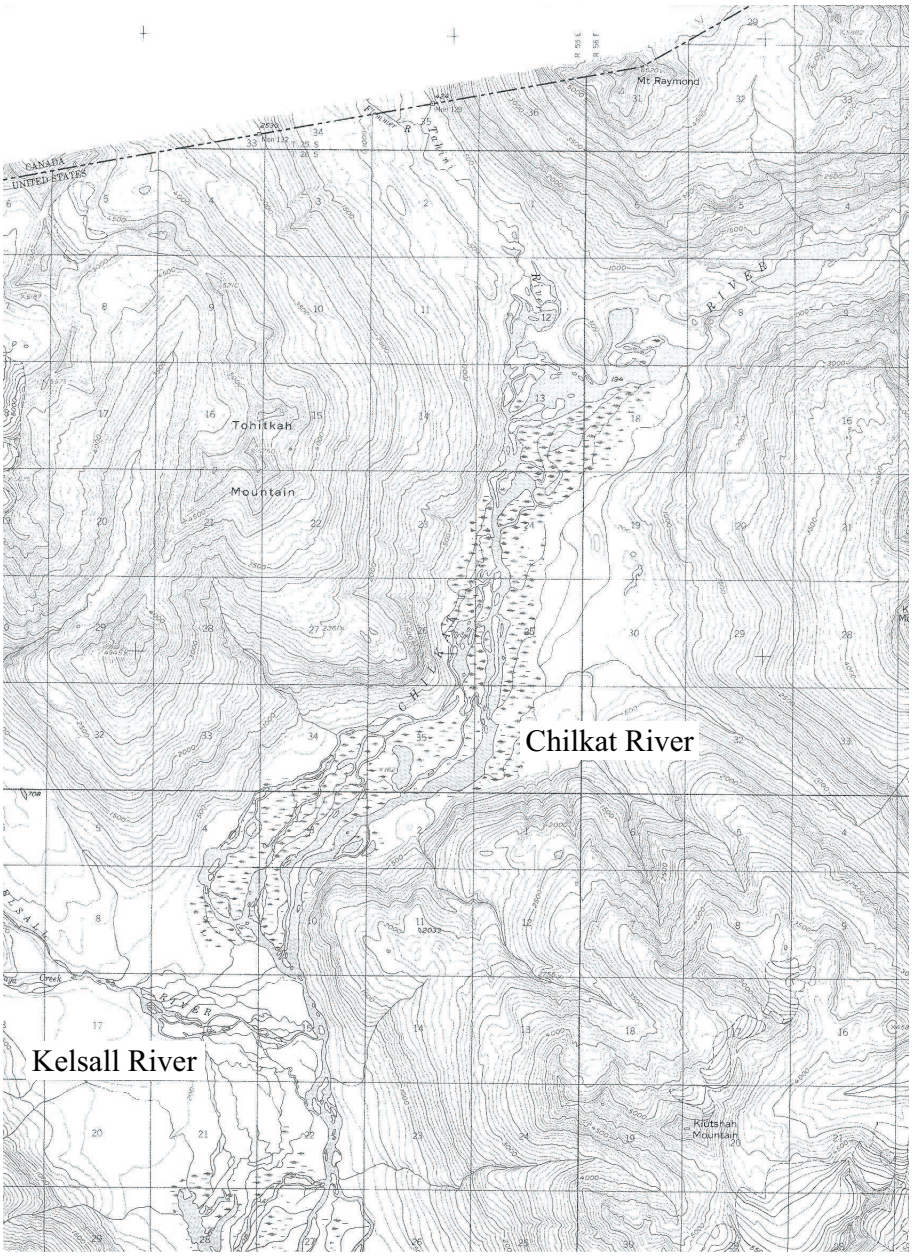

Figure 2.2: Topographic closeup view of region (a) from Fig. 2.1. Source: USGS 7.5 minute Skagway B-3 & C-3 quadrangles.

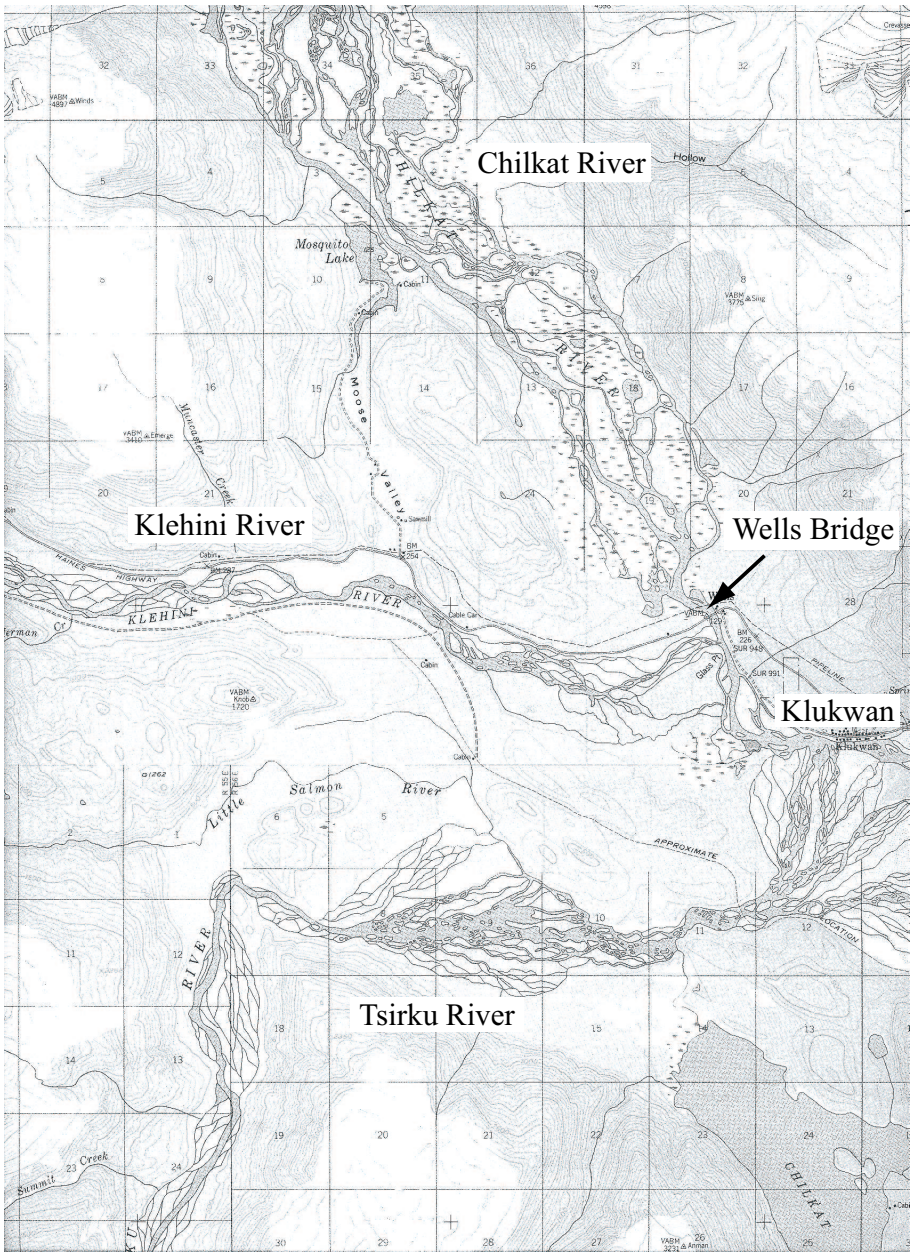

Figure 2.3: Topographic closeup view of region (b) from Fig. 2.1. Source: USGS 7.5 minute Skagway B-3 & C-3 quadrangles.

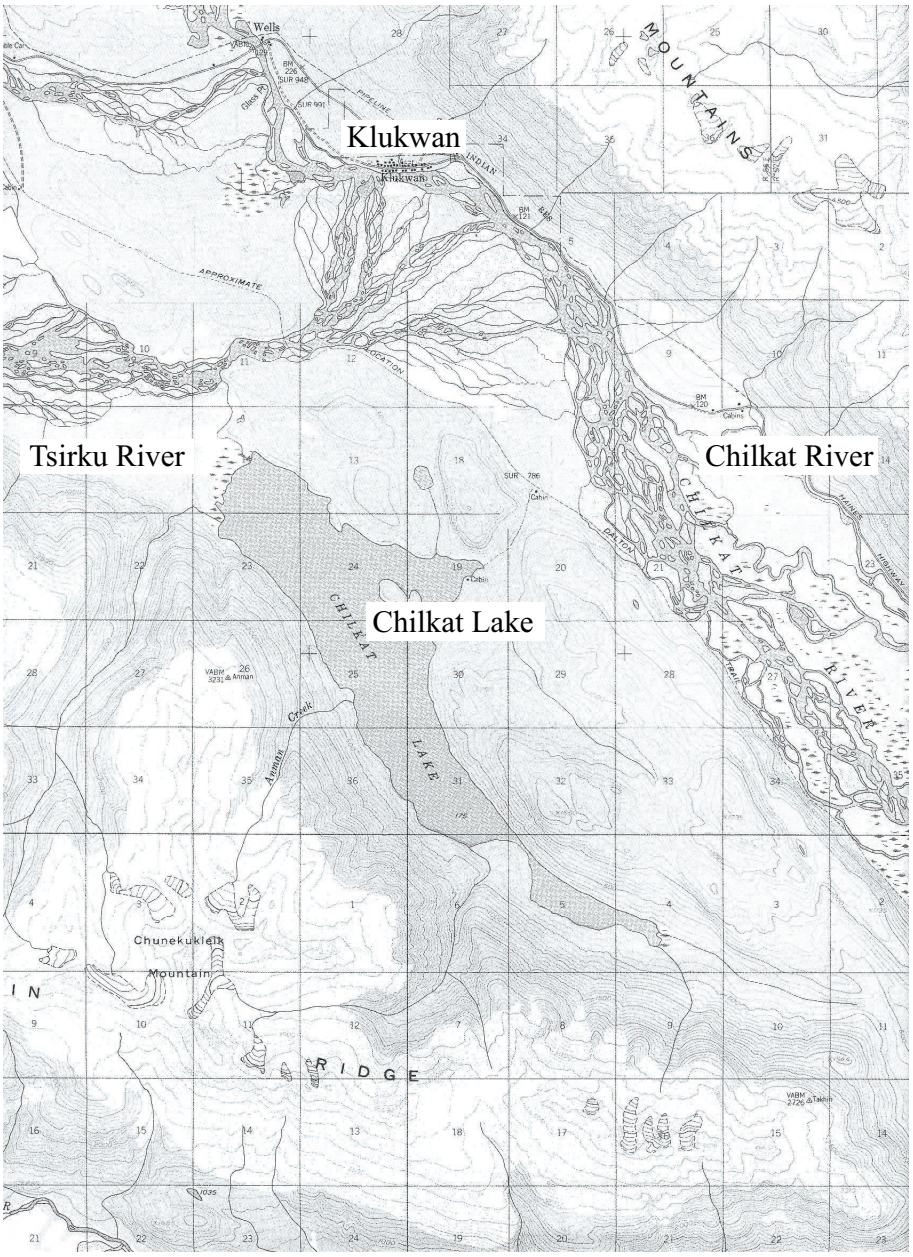

Figure 2.4: Topographic closeup view of region (c) from Fig. 2.1. Source: USGS 7.5 minute Skagway B-3 & C-3 quadrangles.

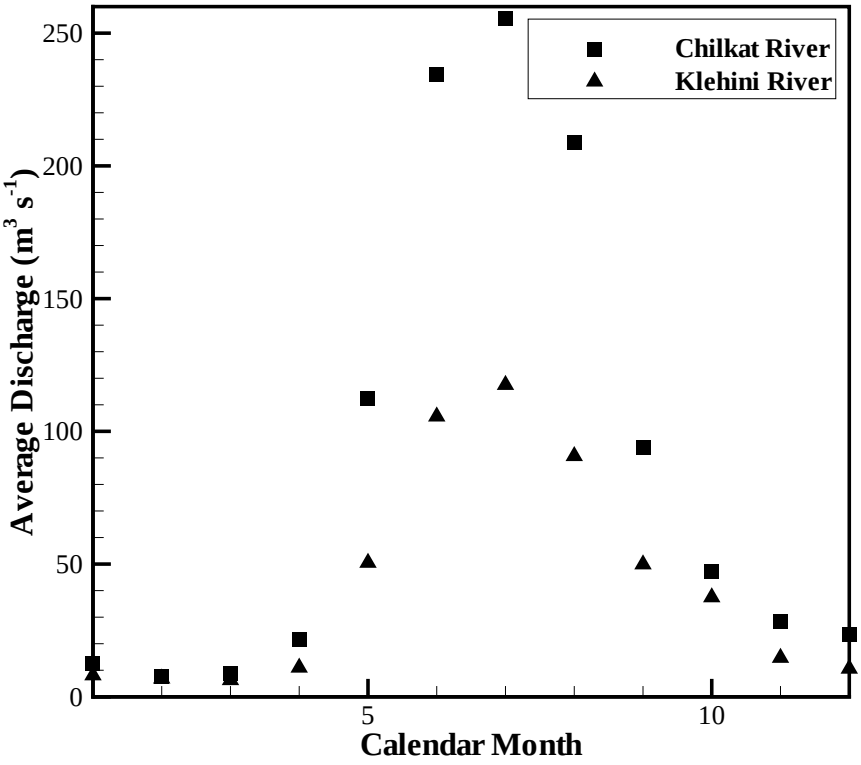

Figure 2.5: Hydrograph for Chilkat and Tsirku Rivers. The data for the Chilkat are for the period from July, 1959 to September, 1961. The data for the Klehini are for the period from October, 1981 to September, 1993. All data are from the U.S.G.S.

2.2 Chilkat River Boat Usage Data

The upper Chilkat River is fairly pristine in that most of the land is public and there is little development. As a result, use levels are comparatively low. To cite a counter example, Dorova and Moore (1997) report that, during a two month summer period on the Kenai River, Alaska, more than 20,100 boats were observed to pass a particular site. Most of these boats were between 5 and 6 m in length and most carried 4 to 5 passengers. Additionally, there is a regulation in place on the Kenai limiting most users to a maximum engine horsepower of 35.

On the upper Chilkat, there is some private boat use, but the majority of the use comes from a commercial tour operator and from employees of the Alaska Department of Fish and Game (ADFG). Regarding the commercial boats, the fleet includes boats that range between 6 and 10 m in length. Passenger loadings on the commercial tours range from 6 to 30 and the horsepower ranges from 180 to 300. Regarding ADFG, their fleet is comprised of boats typically 5 m in length. Horsepower spans the range from 35 to 90 and passenger loading is typically 1 to 2. All boats are described in greater detail in Chapter 4.

While data on private use are not available, some data on commercial use are available from the Alaska Department of Natural Resources. These data indicate that during the 1999, 2000, and 2001 summer seasons, the commercial operator conducted a total of 539, 683, and 473 tours respectively. These numbers will be revisited in Chapter 6, when estimates of boat wake energy are compared to the tractive energy of the river.

2.3 Review of Boat Impact Studies

The potential impacts of watercraft fall into the categories of fuel and exhaust emissions, noise pollution, direct contact with flora and fauna, and hydrodynamic impacts such as wake-induced shoreline erosion and turbulent prop wash. Useful reviews are given by Liddle and Scorgie (1980), Wagner (1991), and WHOI (1998). Attention here will be restricted to hydrodynamic impacts.

2.3.1 Wakes

As an example of hydrodynamic impacts, note first that wakes generated by boat traffic can grade and redistribute sediment (Kirkegaard *et al.*, 1998; Parchure *et al.*, 2001; Parnell and Kofoed-Hansen, 2001). Johnson (1994) correlated boat waves to an increase in shoreline erosion and stirring of bottom sediments in the Upper Mississippi River System (UMRS). Additional work by Bhowmik *et al.* (1992) in the UMRS considered the evolution of a wake packet as it propagated away from the sailing line. An empirical equation was developed in order to predict the wave height as a function of boat size, speed, weight, and distance from the sailing line.

Two recent studies are of particular interest as they specifically consider wake impacts on Alaskan waters. The first study (Dorova and Moore, 1997) made simultaneous measurements of near-bank wave height and 'swash load' at several stations along the Kenai River, which is characterized by very heavy boating use. The latter quantity was estimated by measuring the mass of sediment that was swept into a collection pan mounted on the river bottom near the bank. Additionally, erosion 'pins' were installed at several bank locations. One of the main conclusions was that sediment disturbance near the bank was markedly increased for wake heights exceeding 13-14 cm. By estimating the wake energy dissipated against the banks and the tractive energy of the river flow, it was concluded that the wakes contributed a significant amount of bank erosion at some of the study sites.

Maynord (2001) conducted a thorough set of controlled experiments on the Kenai River and Johnson Lake. The aim of this study was to document the wake characteristics for a wide variety of boat sizes, types, and loadings. Among the conclusions were that (i) wave height increases with passenger loading, (ii) flat-bottomed hulls produce smaller waves than 'V' hulls, and (iii) larger engines can sometimes yield smaller waves for a given hull.

2.3.2 Prop / Jet Wash

Turbulence produced by prop wash has numerous potential impacts as well. The mortality rate of fish eggs due to turbulence was investigated by Killgore *et al.* (1987). Similarly, Morgan *et al.* (1976) studied the mortality rates of perch eggs due to boat-induced shear stress in the Chesapeake and Delaware Canals. Finally, Sutherland and Ogle (1975) exposed salmon eggs to forces equivalent to those induced by passing boats, concluding that jet

boats operating in very shallow rivers could cause substantial mortality.

Prop wash also plays a role in resuspending bottom sediments. This may lead to erosion, internal nutrient loading, or elevated levels of turbidity and heavy metals in the water column. For example, Hamill *et al.* (1999) have studied the 'scour' patterns that develop due to displacement vessels operating in shallow water. Yousef *et al.* (1980) clearly demonstrated increases in nutrient levels in response to boat stirring in Florida lakes. Arruda *et al.* (1983) and Breitburg (1988) both discussed how aquatic wildlife feeding patterns could be disrupted by elevated turbidity levels. Finally, Francisco *et al.* (1999) have identified commercial ferry traffic as the main source of resuspension of contaminated sediments in Elliot Bay, Seattle.

Several investigators have considered the mechanics of bottom stirring by boats. For example, Herbich (1984) used basic momentum conservation and incipient sediment motion relations in his discussion of propeller-induced resuspension. However, few examples were given and no data were cited for comparison. Gucinski (1982) conducted scale-model laboratory experiments of propeller flows in order to complement field observations of boat-induced turbidity in the Chesapeake Bay. His tentative conclusions were that boat-induced resuspension can occur in depths less than 3 meters, but is likely to be of minor consequence until depths are 2.2 meters or less. He further notes that smaller, planing boats will have much less impact than heavy, displacement (deeper draft) boats.

Yousef *et al.* (1978) used pressure sensors to measure the hydrodynamic signal of boat passage at the level of the lake bed. Their observations were incorporated into an empirical design procedure predicting the 'critical' depth of operation, based upon sediment grain size and boat power. Finally, Maynord (1998) provides some useful analysis of propeller flows and bottom shear stress, albeit in the context of larger displacement vessels.

Very recently, Beachler and Hill (2002) conducted a field study aimed at making direct and coupled measurements of the near-bed velocity and turbidity induced by passing watercraft in shallow water bodies. In addition, a simple hydrodynamic model of the flow beneath passing boats was developed in an attempt to be able to predict the onset of sediment motion. The observations and predictions were found to agree reasonably well.

Chapter 3

Water Wave Mechanics

The subject of water waves is very well studied. Many of the fundamentals can be found in texts such as Lamb (1932). For the benefit of the reader lacking a background in waves, the basics will be briefly reviewed here.

3.1 Definitions and General Characteristics

Water waves are disturbances to the equilibrium (i.e. flat) state of the air-water interface, possessing both spatial and temporal periodicity. If a photograph of a wave train were taken, it would look similar to Fig. 3.1, which is an idealized sketch of a wave in water of depth h. Note that x and z here denote horizontal and vertical coordinates.

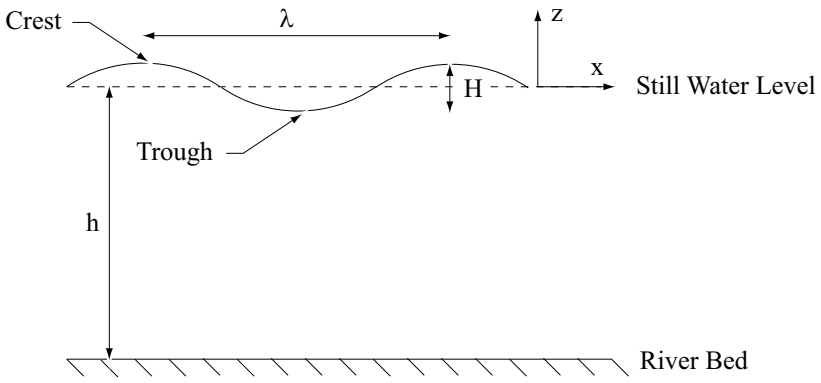

Figure 3.1: A cartoon representation of a water wave.

The disturbance is characterized by an elevation (crest) and a depression (trough) in the water surface. The total vertical distance between these two points is called the wave height, H. The horizontal distance from one crest to the next crest, or from one trough to the next trough, is called the wavelength λ. The wavenumber, k, of a wave is defined as $2\pi/\lambda$ and therefore has units of m^{-1}. The wavenumber can be though of as the spatial 'frequency' of a wave.

If, rather than taking a photograph, which gives a picture at one instant in time, an observer stared at a fixed point in space as a series of waves came by, (s)he would see the wave pattern repeat itself as time passed. The elapsed time from one crest to the next is called the period, T, of the wave. The temporal frequency, ω, of the wave is defined as $2\pi/T$ and therefore has units of s^{-1}. An additional parameter of importance is the celerity, or speed, of a water wave. This is given by $c \equiv \omega/k = \lambda/T$.

The wavenumber and frequency of a wave are uniquely related by what is called a dispersion relationship, given by

$$\omega^2 = gk \tanh(kh),$$

where g is the gravitational acceleration. This equation is easily recast as

$$2\pi\lambda = gT^2 \tanh\left(\frac{2\pi h}{\lambda}\right).$$

The consequence of this relationship is that waves of different wavelengths have different periods. For example, in water of 2 m depth, a wave with a period of 2 s has a wavelength of 6.1 m, while a wave with a period of 1 s has a wavelength of 1.6 m.

Making use of these relationships, the wave speed can be expressed as

$$\begin{aligned} c &= \left[\frac{g \tanh(kh)}{k}\right]^{1/2} \\ &= \left[\frac{g\lambda \tanh(2\pi h/\lambda)}{2\pi}\right]^{1/2}, \end{aligned}$$

with the conclusion that, just as waves of different wavelengths have different periods, they have different speeds as well. This is where the term 'dispersion' comes from. If a wave train consists of many waves of different wavelengths, then, as time goes on, the different waves will move at different

speeds, resulting in the spreading out, or 'dispersion' of the group of waves. This is readily observed when ones throws a rock into a still body of water. The initial splash creates waves of many wavelengths, but the longer, lower frequency waves quickly move out to the front of the spreading rings radiating from the source of impact.

Considering the numerical example from above, the 2 s wave will have a wave speed of 3.02 m s^{-1}, while the 1 s wave will have a wave speed of 1.56 m s^{-1}.

3.2 Velocities, Energy, and Forces

As a water wave propagates through a body of water, it induces motion in the water itself. This is illustrated in Fig. 3.2. The vectors show, at some particular instant in time, the speed and direction of the water in response to a wave moving from left to right. Perhaps the most important point to note is that the velocity decays away from the air-water interface. Indeed, if the water is deep enough, the bottom of a lake or river will not even feel the passage of a wave overhead.

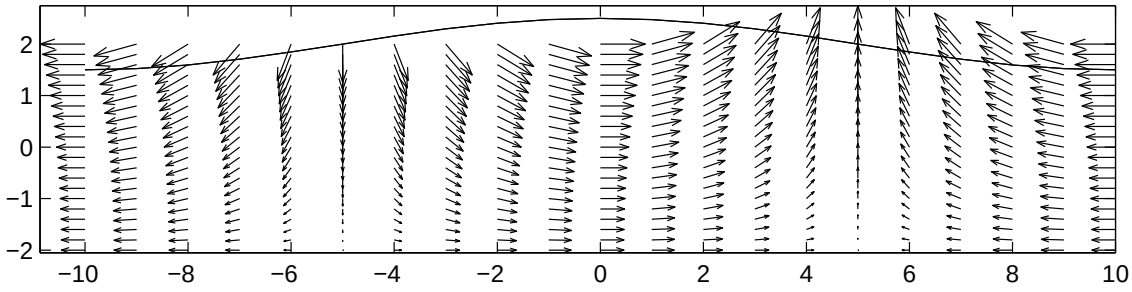

Figure 3.2: Velocity vectors associated with a passing wave. The wave is moving from left to right.

At any given point, the magnitudes of the horizontal and vertical velocity components are given by

$$u = \frac{H\omega}{2}\frac{\cosh[k(z+h)]}{\sinh(kh)}$$
$$w = \frac{H\omega}{2}\frac{\sinh[k(z+h)]}{\sinh(kh)}.$$

Of particular interest, from a sediment transport and 'impact' point of view, the horizontal velocity at the bed (i.e. $z = -h$) of the lake or river has a magnitude of

$$u_b = \frac{H\omega}{2\sinh(kh)}.$$

Returning once more to our example, and assuming a wave height of 50 cm, it is found that the maximum water velocity at the bed is only 1 mm s^{-1} for the 1 s wave. However, for the 2 s wave, the maximum water velocity at the bed is 20 cm s^{-1}, which is high enough to disturb fine to medium sediment grains.

Water waves can possess significant amounts of energy. In the case of boat-generated waves, this energy is supplied by the boat itself. Indeed, wave-resistance is a significant sink of energy for boats. The energy contained in water waves is equally divided between kinetic and potential components. The first of these is associated with the velocity induced in the water. The second is associated with the change in elevation of the water as a wave passes by. The amount of energy, per unit horizontal area, contained in a wave is given by

$$E = \frac{\rho g H^2}{8}.$$

To calculate the *actual* amount of energy in a wave, this figure must be multiplied by the wavelength of the wave and by the breadth of the wave. An important observation is that wave energy is strongly sensitive to wave height. A factor of two increase in wave height leads to a factor of four increase in wave energy.

A related concept is that of wave power. Waves typically propagate until they reach the perimeter of a lake of the bank of river, at which point they break and dissipate their energy. Therefore, from an impact point of view, it is useful to be able to calculate the rate at which this energy is expended. The power, P, in watts, per unit breadth of wave crest, is given by

$$P = E \cdot c \cdot \frac{1}{2}\left[1 + \frac{2kh}{\sinh(2kh)}\right]. \tag{3.1}$$

Finally, in the case of very steep banks and / or a seawall, waves may impact the barrier (Fig. 3.3) and reflect back into the water body, creating a standing, or partially standing, wave. In this case, significant forces can be exerted on the barrier. The magnitude of this force varies throughout the

period of the wave, but the maximum force, per unit length of the barrier, can be estimated from

$$F_{max} = \frac{\rho g h^2}{2} + \frac{\rho g H}{2k} \tanh(kh).$$

Note that the first term is the regular hydrostatic force that exists in the absence of the wave. The second additional term is due to the dynamic loading of the wave.

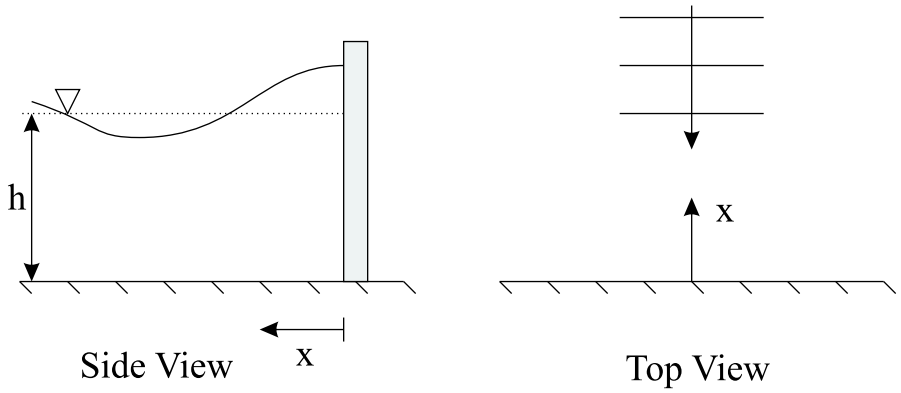

Figure 3.3: Water wave hitting and reflecting from steep vertical barrier.

3.3 Boat Waves

Here, the reader is referred to Sorenson (1973a), Sorenson (1973b), Kirkegaard *et al.* (1998), Stumbo *et al.* (1999), or a report by the Maritime and Coastguard Agency (MCA, 2001) for useful overviews. As a boat travels, it generates a pressure disturbance at the free-surface of the water. This leads to the radiation of waves away from the source, i.e. the boat. The specific nature of the pattern of waves depends upon, among other things, the boat speed, the water depth, and the boat length.

In deep water (Fig. 3.4), there are two sets of oblique diverging waves and a single set of transverse waves, which move in the direction of the disturbance. The 'envelope' that contains the waves is described by a triangle with a half-angle α of 19.3°. This pattern generally agrees with observations in deep water, but some discrepancies do arise since the theory assumes that

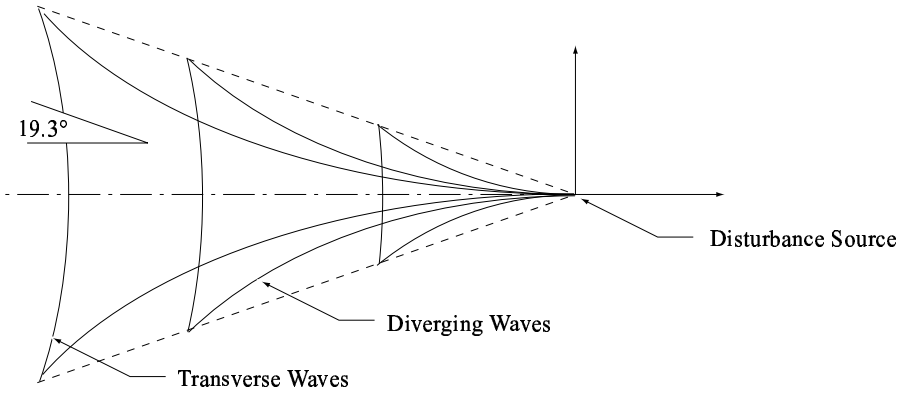

Figure 3.4: Wave crest pattern generated in deep water by a moving pressure disturbance.

the pressure disturbance is concentrated at point while, in reality, boats have finite length.

As a boat moves into shallower water, the waves begin to be influenced by the depth. While the transition is gradual and, therefore, no sharp boundary between deep and shallow water exists, it is generally accepted that the water is deep when $h/\lambda > 0.5$. This boundary can also be expressed in terms of the 'depth-based' Froude number, $Fr_d \equiv V_b/(gh)^{1/2}$, of the boat, where V_b is the boat's speed. For values of Fr_d greater than about 0.6 to 0.7, the waves will 'feel' the presence of the bottom.

Once this begins to happen, the half-angle of the envelope containing the waves begins to increase, up to a value of 90° when $Fr_d = 1$. Further increases in Fr_d result in decreases in α.

Two items of particular interest to the present study are (i) how the maximum wave height in a train of boat waves varies with Fr_d and (ii) how the maximum wave height in a train of boat waves diminishes with distance from the sailing line of the boat.

Regarding the first point, numerous studies (Sorenson, 1973a; Byrne *et al.*, 1980; Kirkegaard *et al.*, 1998) have demonstrated that wave heights are strongly controlled by Fr_d, with a significant peak at $Fr_d \sim 1.0$. This has practical implications, from a management point of view. For example, Parnell and Kofoed-Hansen (2001) discuss the management of high-speed ferries in confined coastal waters in Denmark and New Zealand. To minimize the safety hazards and environmental impacts of wake wash, it is desirable to

minimize the amount of time that a vessel spends travelling at the 'critical' speed $(gh)^{1/2}$.

The length of a boat also plays a role in determining how large the generated wakes are (Parnell and Kofoed-Hansen, 2001; MCA, 2001). This leads to the definition of a second Froude number, the 'length-based' Froude number $Fr_l \equiv V/(gL)^{1/2}$, where L is the boat length. Studies have shown that when $Fr_l \sim 0.5$, wave heights are once again maximized. Combining these two concepts, it is seen that a worst-case scenario exists where the boat speed, length, and water depth are such that both Froude number criterion are satisfied simultaneously.

Turning to the second point, the maximum wave height, H_{max}, in a wave train will generally diminish as the train propagates away from the sailing line of the boat. This is due to the dispersion effect, discussed earlier. While this rate of decay can, in principle, be determined theoretically, it is generally determined empirically, based upon laboratory or field experiments. The decay is most commonly assumed to follow a power-law relationship such that the maximum wave height at some perpendicular distance x from the sailing line is given by

$$H_{max}(x) \propto x^{-\beta}.$$

Decay coefficients determined in previous studies are summarized in Table 3.1.

Study	β
Bhowmik (1975)	0.46
Maritime Coastguard Academy (2001)	0.25
Maynord (2001), Johnson Lake	0.40
Maynord (2001), Kenai River	0.29

Table 3.1: Experimentally determined decay coefficients for maximum wave heights.

Chapter 4

Experimental Sites, Facilities, & Instrumentation

In this chapter, a detailed description of the study sites, boats, and experimental instrumentation is given.

4.1 Study Sites

Quantitative measurements of boat wake heights, near-bank turbidity and / or near-bottom disturbances were made at a total of six sites during the field study. These sites are indicated in Fig. 4.1, which is a composite aerial photograph of the Upper Chilkat River (above Wells Bridge). Closeup aerial pictures of the sites are provided in Fig. 4.2.

The site selection process was driven by a host of considerations, including the Alaska Department of Fish & Game's (ADFG) concerns about salmon habitat in specific locations, ease of accessibility, and the desire to study wake characteristics under as wide a variety of conditions as possible.

4.1.1 General Characteristics and Observations

The Chilkat River is a braided or partially braided river for much of its length. A braided river is one that is characterized by a highly variable width, a steep slope, rapid rates of lateral migration, and interlacing channels within the main channel, separated by unvegetated mid-channel bars. These channels typically carry a heavy bedload during high flows. In the case of the Chilkat

River, the large bedload originates from upstream glacial activity.

In order to obtain an overall indication of the current morphologic conditions of the Chilkat River, morphologic data were collected during a preliminary visit by the authors in April of 2002. Due to the limited access to the river at this time, only two sites were visited.

The first site was the boat launch referred to informally as the 'Kelsall Landing'. Here, the width was roughly 60 m with a bankfull depth of roughly 1.5 m. The banks consisted of glacially derived cobbles, gravel, and glacial flour. Both banks were nearly vertical and on each bank there was only a single line of old and new growth woody vegetation. There was moderate fluvial erosion and bank cutting. No mass wasting was present, however the occurrence of numerous overhanging banks indicated the potential for mass wasting.

Large bars were present at this location. Some larger, vegetated islands have been stable for more than 40 years based upon the examination of aerial photos. Smaller, unvegetated mid-channel bars consisted of a mix of sand, gravel, and cobbles, with gravel the predominant size. The width of these bars varied widely from 1.5 to 9 m. The larger bars and islands had well established woody vegetation, primarily on the right bank.

A stability analysis was conducted at this site based on a method developed by Johnson *et al.* (1999). This method rates 13 stability indicators to determine the relative stability. The indicators include: bank material, bank angle, vegetative bank cover, fluvial bank cutting, mass wasting, bars, debris potential, flow obstructions, bed material, and shear stress. The overall ranking is assigned a rating of excellent, good, fair, or poor. The result of this analysis showed that the river at this site had a 'fair' rating. This implies that this reach is somewhat unstable. This is to be expected since braided rivers are naturally unstable in that their bars shift frequently and their banks are quite mobile such that lateral changes in width and location are common. This also implies that the braided river is very susceptible to imposed changes, such as changes in hydrology or sediment load.

The second site surveyed on this preliminary visit was approximately 500 m southwest of what is referred to as Jacquot's Landing, which is, in turn, slightly southwest of the confluence of the Kelsall and Chilkat Rivers. At this point on the river, the main channel was about 30 m wide and was a single thread river with a bankfull depth of about 1.3 m. The banks consisted of glacially derived cobbles, gravel, and glacial flour in the upper bank and gravel and cobbles in the lower bank.

Both the left and right upper banks were nearly vertical; the lower banks were sloped at about 45 degrees. Note that 'right' and 'left' are defined with the observer looking downstream, as is the usual convention. The left bank was about 1.2 m high and the right bank was about 1.8 m high. Both overbank areas were forested. The right bank had significant fluvial erosion and bank cutting, undercutting the upper bank by several feet. Fluvial erosion was minimal on the left bank. Mass wasting was minimal on either bank, however the occurrence of overhanging banks on the right bank was indicative of the potential for mass wasting.

A single mid-channel bar existed in this reach. It consisted primarily of gravel and was about 9 m wide. Although the bar was covered with perennial vegetation, there was no woody vegetation; thus, it can be concluded that this would be a mobile bar only under very large hydrologic events. The bed material at this site was primarily sand and fine gravel overlain by coarser gravel.

A stability analysis was conducted at this site based on a the same method developed by Johnson *et al.* (1999). The result of this analysis showed that the river at this site had a 'fair' rating. This implies that this reach is somewhat unstable. Similar to the result the other site, this is to be expected since braided rivers are naturally unstable with frequently shifting bars and mobile banks. The implication is that the braided river is very susceptible to imposed changes, such as changes in hydrology or sediment load.

Observations made at other sites during the main study in May and June of 2002 revealed similar characteristics. An additional observation of note is that of frequent semi-circular 'scallops' (Fig. 4.3) along many of the banks. These scallops, frequently 1-2 m in length (along the bank) and 1 m in width (into the bank), are indicative of banks eroding at a higher than normal rate. Regardless of cause, they represent areas of particular susceptibility.

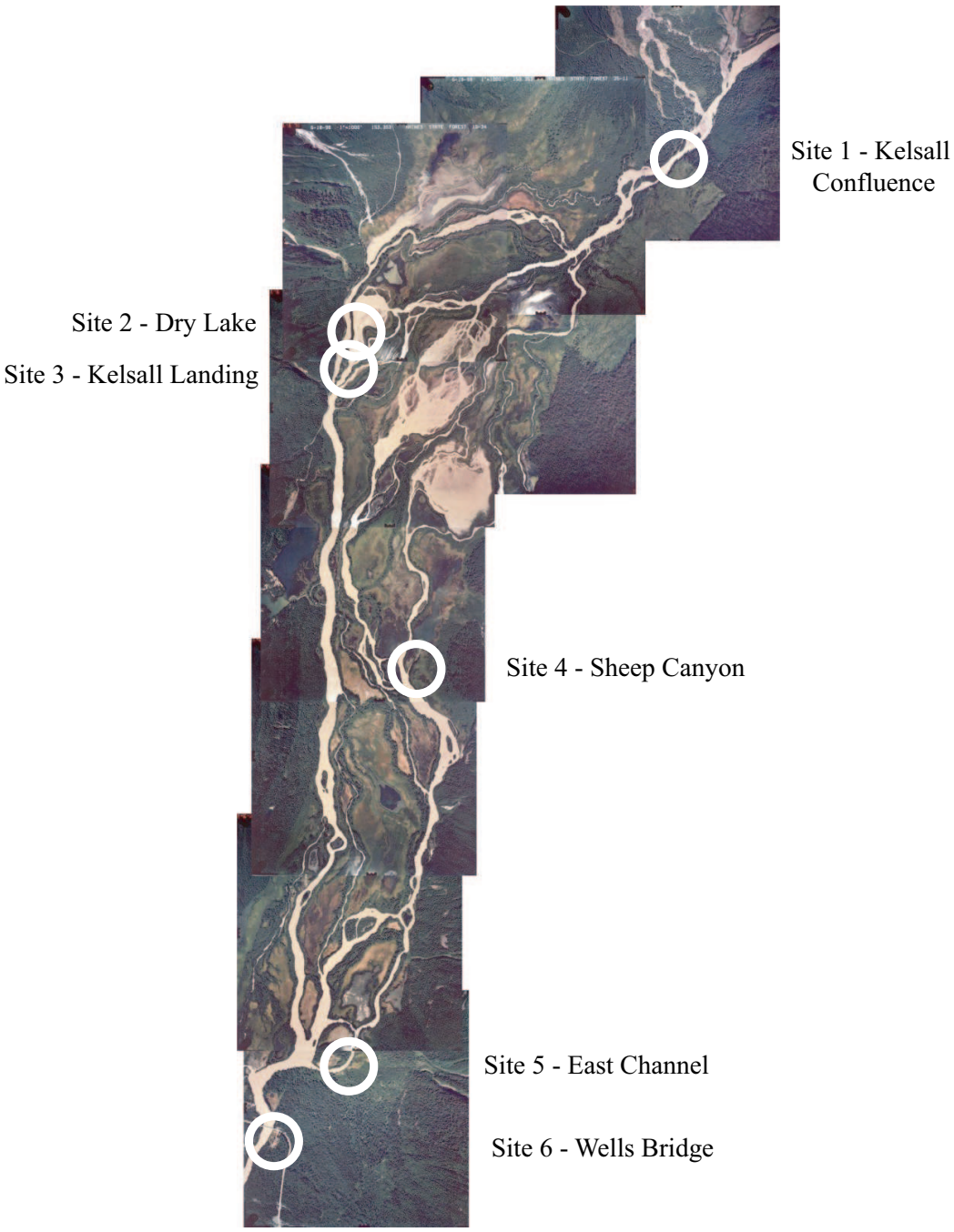

Figure 4.1: Aerial photograph mosaic indicating the six study sites.

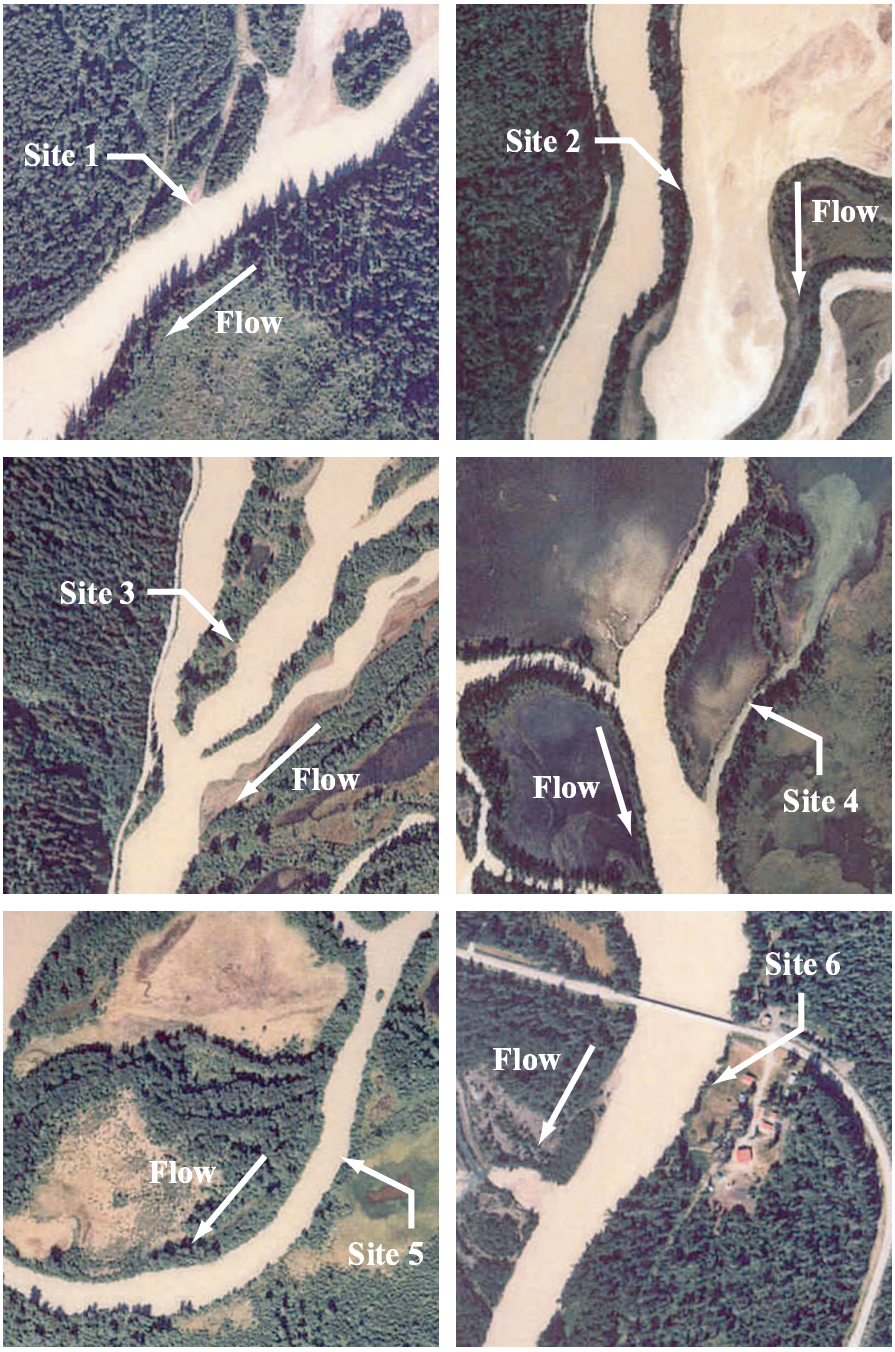

Figure 4.2: Closeup aerial photographs of the six study sites.

Figure 4.3: Small-scale scallops typical of poorly vegetated banks on the Chilkat River.

4.1.2 Specific Site Descriptions

Site 1 - Kelsall Confluence

Site 1 lies slightly upstream of Jacquot's Landing and slightly downstream of the confluence of the Kelsall and Chilkat Rivers. Instrumentation was set up on the right bank, in-between two small clear-water inflows. The banks at this location were heavily scalloped (Fig. 4.4). At this location, the entire flow of the upper Chilkat is confined to a single channel. The width of the channel was approximately 70 m, the maximum depth was not measured. Due to the high flows in the channel, wading discharge measurements were not feasible. However, measurements of surface drift velocity were made in the middle of the channel with a GPS unit and indicated a velocity of approximately 2.2 m s^{-1}.

Figure 4.4: Right bank, showing the location of study site.

Site 2 - Dry Lake

Site 2 was just downstream of what is known as Dry Lake. This site was selected due to the exposed nature of the banks (Fig. 4.5) and the observed proximity of the boats to the right banks. Instrumentation was set up on

the right bank. The width of the channel at this location was approximately 125 m and the maximum depth was approximately 1.5 m. This depth precluded a wading survey and discharge calculation, but such measurements were possible about 100 m downstream (Fig. 4.6).

Figure 4.5: Right banks downstream of Dry Lake.

At this location, the discharge was 73.1 $m^3\ s^{-1}$, the cross-sectional area was $A = 126.2\ m^2$, and the wetted perimeter was $\mathcal{P} = 164.3$ m, yielding a hydraulic radius of $R_h = 0.77$ m and an average velocity of $\overline{V} = 0.58\ m\ s^{-1}$.

Site 3 - Kelsall Landing

Site 3 (Fig. 4.7) was slightly downstream of Dry Lake and slightly upstream of what is informally referred to as the Kelsall Landing. At this location, the channel splits into three stems and the study site was on the right bank of the middle stem. This site was the most heavily studied as its size and flow characteristics were ideal for the installation of a maximum amount of instrumentation.

The width of the channel was approximately 70 m and the maximum depth was approximately 1.5 m, which, as with the Dry Lake site, precluded a complete wading survey. In order to estimate the discharge at the study

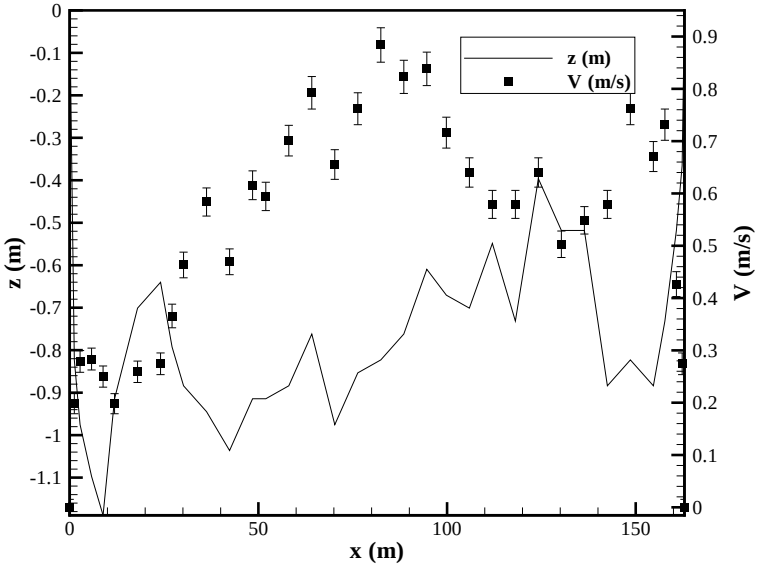

Figure 4.6: Depth and depth-averaged velocity profiles slightly downstream of Site 2 and slightly upstream of Site 3. $x = 0$ refers to the left bank.

site, the discharge of the single tributary between Sites 2 and 3 was measured and added to the discharge measured just downstream of Site 2. The survey measurements in this tributary are shown in Fig. 4.8. The calculated discharge in the tributary was 3.1 m^3 s^{-1}, bringing the total discharge past Site 3 to 76.2 m^3 s^{-1}.

Site 4 - Sheep Canyon

Site 4 (Fig. 4.9) was located off what is called the 'east channel' of the upper Chilkat. The site was on the right bank of a narrow clear-water channel connecting what is referred to as Sheep Canyon Lake to the east channel of the Chilkat River. This site was selected for two major reasons. First of all, it was the smallest, lowest-flow channel (Fig. 4.10) on the route run by the commercial operator. As such, the conditions were favorable for initial testing of the instrumentation. Second, the site is the source of a recent management decision by ADFG. Previously, the operator was permitted to navigate the channel 'on step', at speeds exceeding 20 miles per hour. Due to concerns about bank erosion, ADFG recently restricted the operator to 'slow-no wake' operation. The hope of the authors was that measurements

Figure 4.7: Looking upstream from the middle of the channel at Site 3.

would help to shed light on the appropriateness of the management action.

At this site, the width of the channel was approximately 15 m and the maximum depth approximately 1.2 m. The discharge was found to be $Q = 1.0$ m^3 s^{-1}, the cross-sectional area was $A = 13.6$ m^2, and the wetted perimeter was $\mathcal{P} = 17.1$ m, yielding a hydraulic radius of $R_h = 0.80$ m and an average velocity of $\overline{V} = 0.074$ m s^{-1}.

Site 5 - East Channel

A limited number of measurements of ADFG boat wakes were made throughout the present study, most of which occurred a site (Fig. 4.11) in the east channel of the upper Chilkat. The cross-channel variation in depth and velocity are shown in Fig. 4.12.

The site was located on the left bank of the channel, which was approximately 45 m wide and had a maximum depth of approximately 1.2 m. The discharge was $Q = 14.0$ m^3 s^{-1}, the area was $A = 29.4$ m^2, and the wetted perimeter was $\mathcal{P} = 46.8$ m, yielding a hydraulic radius of $R_h = 0.63$ m and an average velocity of $\overline{V} = 0.48$ m s^{-1}.

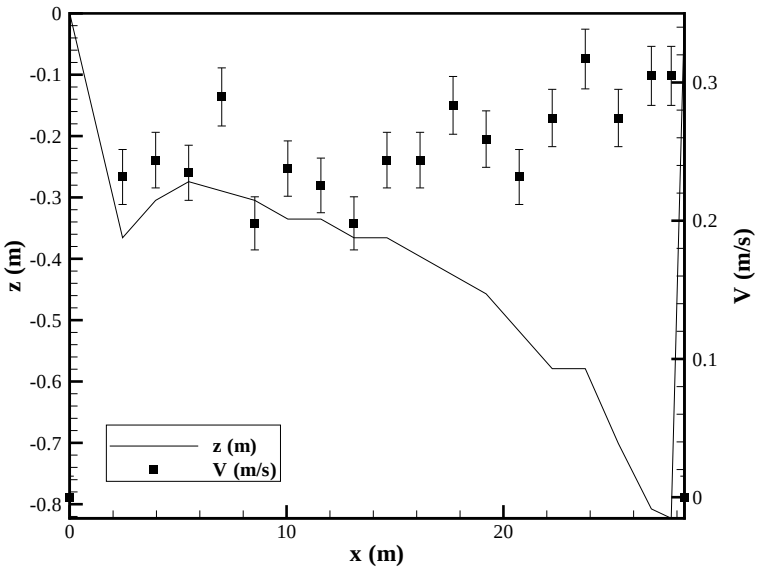

Figure 4.8: Depth and depth-averaged velocity profiles in small tributary just upstream of study site. $x = 0$ refers to the left bank.

Site 6 - Wells Bridge

Finally, a very limited number of measurements were made on the left bank of the river (Fig. 4.13), just below Wells bridge. This site was chosen, due to extreme ease of access, in order to test and troubleshoot the instrumentation during the first few days of the study period. At this location, the width of the river was approximately 150 m, but the maximum depth and the discharge were not measured. However, by totalling up the discharges measured in the various channels upstream, and by making reasonable assumptions about the flows in channels where the discharge was not measured, the discharge past Wells bridge was estimated to be approximately 125 $m^3\ s^{-1}$.

Figure 4.9: Typical banks in the channel leading to Sheep Canyon Lake. Photo by Ben Kirkpatrick.

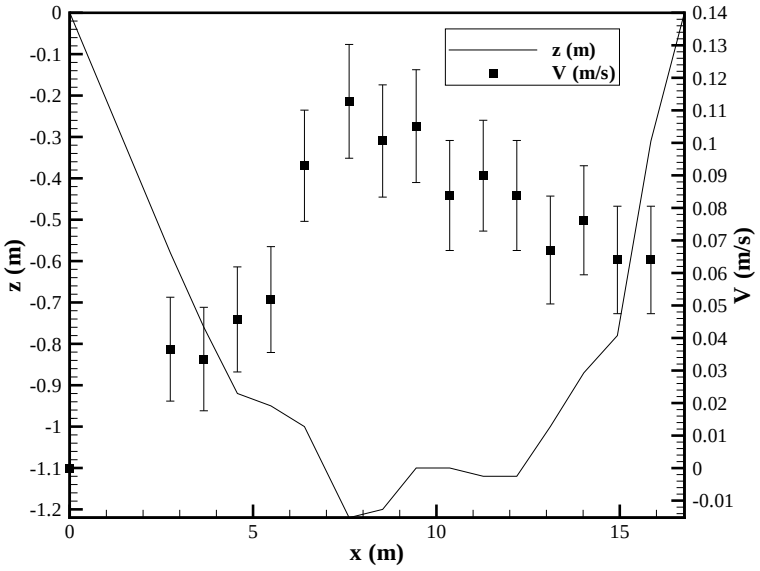

Figure 4.10: Depth and depth-averaged velocity profiles in the clearwater channel connecting Sheep Canyon Lake to the East Channel. $x = 0$ refers to the left bank.

Figure 4.11: View of the east channel, as seen from Site 5, located on the left bank.

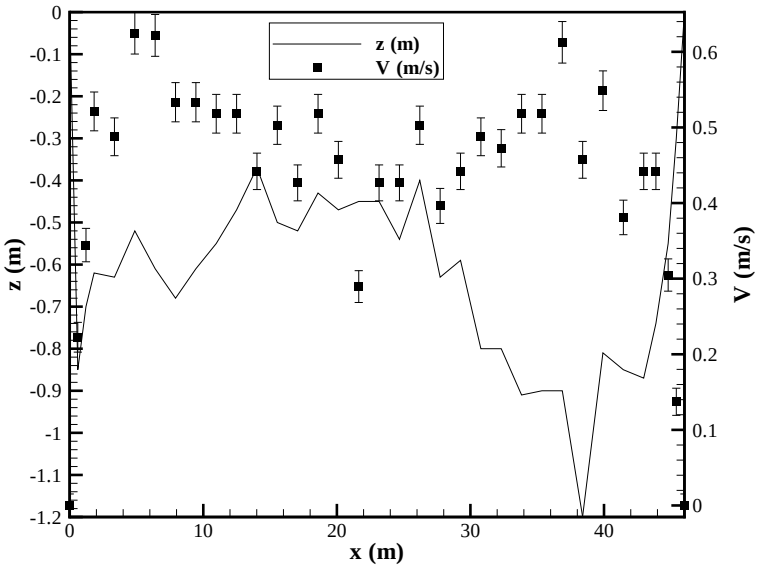

Figure 4.12: Depth and depth-averaged velocity profiles in the East Channel. $x = 0$ refers to the left bank.

Figure 4.13: A set of wakes approaching Site 6, on the left bank of the river.

4.1.3 Sediment Characteristics

With the exception of Site 6, a small bank-material sample was taken at each study site. These samples were later analyzed in order to obtain basic engineering properties such as grain size distribution and liquid limit. Based upon these properties, it was then possible to assign a two-letter designation, as outlined by the Unified Soil Classification. This classification scheme, widely used in geotechnical engineering, is summarized in Table 4.1.

Beginning first with the grain size analysis, seven sieves (# 4, 8, 16, 30, 50, 100, and 200) were used to partition the dry samples. The distribution curves for for five sites sampled are given in Fig. 4.14. From these curves, the median grain sizes were determined and are summarized in Table 4.2. In the cases where more than 50% of the sample was finer than the finest sieve used (75 micron mesh), the exact value of d_{50} could not be determined.

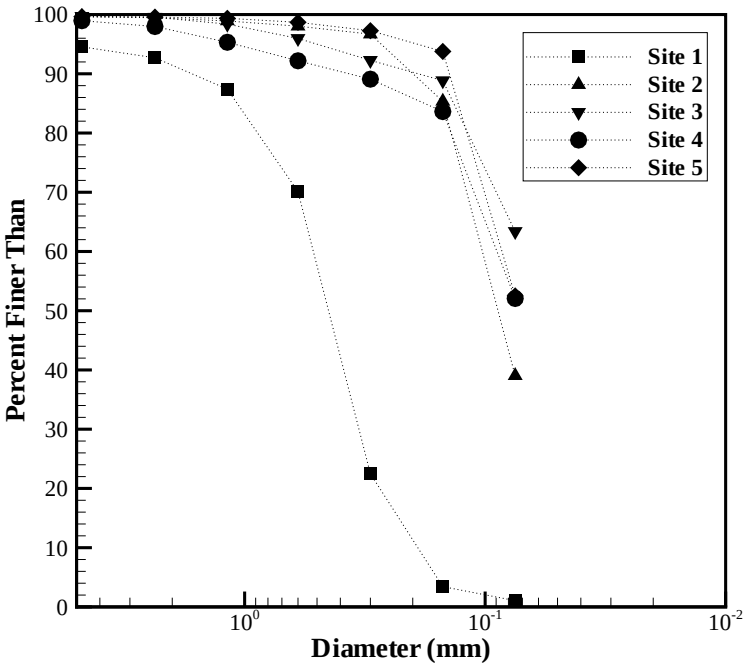

Figure 4.14: Grain size distributions for Sites 1-5.

Next, the liquid limit was determined, when possible. As explained by Derucher *et al.* (1994), this is defined as the water content above which the soil behaves as a viscous liquid. For Sites 2-4, the liquid limit was found to be

in the range of 20 to 25. Based upon this information, and the median grain diameters, the soil samples from the various sites were classified as outlined in Table 4.3.

Major Divisions			Group Symbols	Typical Names
Coarse-Grained Soils, More than 50% retained on No. 200 Sieve	Gravels, ≥50% of coarse fraction retained on No. 4 sieve	Clean Gravels	GW	Well-graded gravels and gravel-sand mixtures, little or no fines
			GP	Poorly graded gravels and gravel-sand mixtures, little or no fines
		Gravels with Fines	GM	Silty gravels, gravel-sand-silt mixtures
			GC	Clayey gravels, gravel-sand-clay mixtures
	Sands, ≥50% of coarse fraction passes on No. 4 sieve	Clean Sands	SW	Well-graded sands and gravelly sands, little or no fines
			SP	Poorly graded sands and gravelly sands, little or no fines
		Sands with Fines	SM	Silty sands, sand-silt mixtures
			SC	Clayey sands, sand-clay mixtures
Fine-Grained Soils, 50% or more passes No. 200 Sieve	Silts and Clays, Liquid Limit 50% or less		ML	Inorganic silts, very fine sands, rock flour, silty or clayey fine sands
			CL	Inorganic clays of low to medium plasticity, gravelly clays, sandy clays, silty clays, lean clays
			OL	Organic silts and organic silty clays of low plasticity
	Silts and Clays, Liquid Limit greater than 50%		MH	Inorganic silts, micaceous or diatomaceous fine sands or silts, elastic silts
			CH	Inorganic clays of high plasticity, fat clays
			OH	Organic clays of medium to high plasticity
Highly Organic Soils			PT	Peat, muck, and other highly organic soils

Table 4.1: Unified Soils Classification (USC), adapted from Derucher *et al.* (1994).

Site	d_{50} (mm)
1	0.47
2	0.093
3	< 0.075
4	< 0.075
5	< 0.075

Table 4.2: Median grain sizes (d_{50}) for the study sites.

Site	USC Code
1	SP
2	SM or SC
3	ML or CL
4	ML or CL
5	ML or CL

Table 4.3: USC designation for bank material from the six study sites.

4.2 Descriptions of Boats and Motors

During the course of this study, quantitative measurements of six different boats were made. Four of the boats belonged to the commercial operator and two belonged to ADFG. All of the boats were powered by outboard jet-drive motors. As illustrated in Fig. 4.15, a jet-driven outboard motor is identical to a propeller-driven outboard motor, with the exception that the lower unit has been replaced by an impeller. The foot of the impeller is generally configured to be flush with or slightly extend below the bottom of the boat. The net effect of this is that jet-driven boats are capable of navigating in extremely shallow (less than 25 cm) water.

Figure 4.15: Jet-drive outboard motor.

In addition to possessing jet-drive motors, a common characteristic of boats on the upper Chilkat River is that they usually have flat-bottomed or semi-V hull shapes. This minimizes the draft of the boats and helps them to get on plane more rapidly.

The smallest boat tested (Fig. 4.16), *FG16*, was a MonArk (model # 10-10-1652) river boat. The length of this boat was 4.84 m and the beam at the transom was 1.85 m. The boat was powered by a 50 hp Yamaha engine. The mass of the hull was approximately 125 kg and the mass of the engine was approximately 85 kg. These figures, and those for the other boats, are summarized in Table 4.4.

Figure 4.16: Photo of *FG16*, the snaller of the ADFG boats tested.

The next largest boat tested (Fig. 4.17), *FG18*, was a Valco (model # RB18STD). The length of this boat was 5.60 m and the beam at the transom was 1.49 m. The boat was powered by a 90 hp Yamaha engine. The mass of the hull is 143 kg and the mass of the engine was approximately 120 kg.

The remaining four boats were part of the commercial operator's fleet. All were flat-bottomed, modified Carolina skiffs. Due to limited access to the boats, only rough data are available for the specifications. For example, to estimate the weights of the hulls, weight vs. length data were taken from the Carolina Skiff website. A straight-line was fit to the data, as illustrated in Fig. 4.18, and the equation of the line was used to estimate the weights of the boats in the fleet.

The smallest of the commercial boats (Fig. 4.19), *COM20*, had a length of 6.1 m, a beam of 2.1 m, and was powered by twin 90 hp engines. The mass of the hull was approximately 494 kg and the combined mass of the engines was 240 kg.

Next, *COM24* (Fig. 4.20) had a length of 7.3 m, a beam of 2.1 m, and was powered by twin 115 hp engines. The mass of the hull was approximately

Figure 4.17: Photo of *FG18*, the larger of the ADFG boats tested.

660 kg and the combined mass of the engines was 325 kg.

Third, *COM28* (Fig. 4.21 had a length of 8.5 m, a beam of 2.1 m, and was powered by twin 115 hp engines. The mass of the hull was approximately 825 kg and the combined mass of the engines was 325 kg.

Finally, the largest boat (Fig. 4.22) in the fleet, *COM32*, had a length of 9.8 m, a beam of 2.4 m, and was powered by twin 150 hp engines. The mass of the hull was approximately 995 kg and the combined mass of the engines was 390 kg.

Boat	Length (m)	Beam (m)	Engine HP	Engine Mass (kg)	Hull Mass (kg)
FG16	4.84	1.85	50	85	125
FG18	5.60	1.49	90	120	143
COM20	6.1	2.1	180	240	494
COM24	7.3	2.1	230	325	660
COM28	8.5	2.1	230	325	825
COM32	9.8	2.4	300	390	995

Table 4.4: Summary of specifications of boats studied.

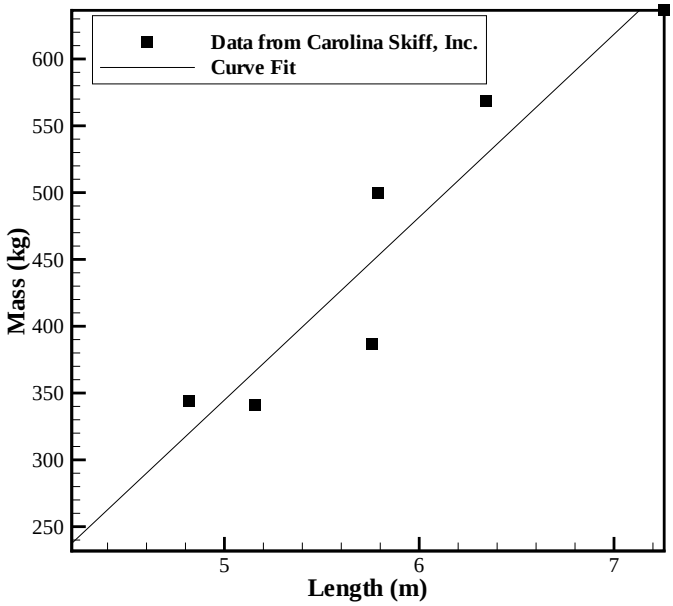

Figure 4.18: Boat mass data taken from Carolina Skiff specifications. The best-fit straight line is also shown.

Figure 4.19: Photo of *COM20*, the smallest of the commercial boats studied.

Figure 4.20: Photo of *COM24*, the second-smallest of the commercial boats studied.

Figure 4.21: Photo of *COM28*, the second-largest of the commercial boats studied.

Figure 4.22: Photo of *COM32*, the largest of the commercial boats studied.

4.3 Instrumentation

4.3.1 Velocity Measurements

To measure the water velocity induced underneath the passing boats, a SonTek 10 MHz acoustic doppler velocimeter (ADV) was used. This instrument is shown in Fig. 4.23. The ADV is capable of measuring three components of velocity at sampling rates of up to 20 hertz. The ADV operates by emitting acoustic energy from a transmitter located at the end of the probe. These signals are relected off of tiny particles in the water and scattered back to three receivers. By analyzing the Doppler shift in the frequency, the velocity of the particles, and, by assumption, the carrier water can be deduced. The sampling volume of the ADV is cylindrical in shape, has a volume of approximately 0.3 cm^3, and is located 10 cm away from the tip of the probe. For the measurements reported herein, the ADV was used in a 'side-looking' mode. In this configuration, the ADV was mounted horizontally to a piece of wood that was then laid on the bed of the river. The measurement volume was approximately 10 cm above the bed of the river.

Figure 4.23: Sontek acoustic doppler velocimeter, in 'side-looking' mode.

4.3.2 Turbidity Measurements

To measure the turbidity of the water, an optical backscatter sensor (OBS-3), manufactured by D&A Instrument Company, and powered by a 12 VDC marine battery was used. The instrument is shown in Fig. 4.24.

The instrument operates by emitting infrared light at a 50° maximum angle in the vertical direction and a 30° maximum angle in the horizontal plane, producing a conical sampling volume. The light beams reflect off of

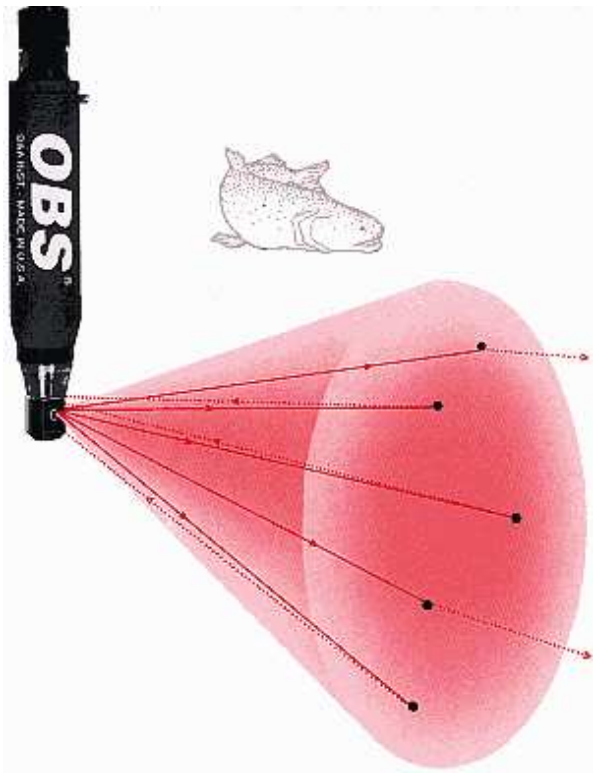

Figure 4.24: Optical backscatter sensor. Source: D&A Instrument Company.

materials suspended in the water column. Some of the scattered light returns to the receiver and is processed. The voltage output of the OBS-3 can be calibrated to turbidity units or, provided a local sediment sample is acquired, to suspended sediment concentration. Details of this procedure can be found in Beachler (2002) and calibration results for the study sites are given in Chapter 5 of the present report.

For most of the measurements reported herein, the OBS-3 was mounted vertically, using a length of re-bar or pipe, in the vicinity of the bank of the river. A more limited number of experiments were performed with the OBS-3 mounted close the bed of the river and directly underneath the passing boats.

4.3.3 Wave Height Measurements

To measure the elevation of the water surface, a total of four capacitance wave gages were used. Two of the units were from Richard Brancker, Ltd., (model # WG-50) and the other two were from Ocean Sensor Systems (model # OSSI010-002C). The two different styles are illustrated in Figs. 4.25-4.26.

Figure 4.25: WG-50 capacitance wave gage, manufactured by Richard Brancker, Ltd.

The WG-50 consists of a thin wire, approximately 1 mm in diameter and 1 m in length, supported by a 'C'-shaped metal bracket. The gage is connected to a splash-proof unit containing the electronics via a 1 m BNC cable. This unit is in turn connected to a 40 m cable running to shore. The OSS gage consists of a flexible rod, approximately 5 mm in diameter and 1 m in length. The rod is directly connected to a small cylindrical unit containing the necessary electronics. This unit is, as with the WG-50, connected to a cable leading to shore.

Both gages operate in the same fashion. An insulated lead with no gal-

Figure 4.26: OSS capacitance wave gage, manufactured by Ocean Sensor Systems.

vanic connection to the water (i.e. the wire / rod) is partially immersed in the water. This, together with a ground connection forms a linear capacitor. As the water surface rises and falls, due to passing waves, the capacitance of the circuit similarly varies. Due to the linearity of the relationship between the two quantities, a simple two-point calibration is sufficient to relate the voltage output of the wave gage to water elevation.

In all cases, the wave gages were mounted by driving a length of iron pipe (2.5 cm diameter) firmly and vertically into the bed of the river. The wave gage was then attached to the pipe using plastic cable ties. To minimize any potential interference with the slight wake created by the pipe, the gage was mounted such that it was upstream or to the side of the pipe. As discussed by Maynord (2001), there are a number of technical challenges in using capacitance gages in rivers with swift currents. The rod-type gages, with their appreciable diameters, may lead to slight errors due to the stagnation rise of water on the upstream surface of the rod. The wire-type gages may frequently break due to the forces induced by the current and by collisions with debris in the river. As the currents experienced in the present study (1 m s^{-1} max) were significantly less than those reported by Maynord (2001) (2-3

m s^{-1}), these difficulties were largely avoided.

4.3.4 Boat Speed Measurements

The method used for measuring boat speed depended upon whether or not the experiments being performed were controlled or uncontrolled. In the case of controlled experiments with ADFG boats, a handheld GPS unit (Garmin Etrex Vista) was used. Despite the ± 0.1 mph precision of this unit, it was estimated that the practical accuracy of the speed measurements was ± 1 mph. This is due to the difficulty in holding a boat, particularly at near-planing speeds, at a constant speed.

For the uncontrolled measurements of the commercial boats, a radar gun (Stalker Sport) was used. Again, while the measurement device possessed a nominal accuracy of ± 0.1 mph, the authors feel that an uncertainty of ± 1.0 mph is more representative. This is due to a variety of reasons. First of all, radar gun measurements are sensitive to the 'line of sight.' In other words, the radar gun should be aligned with the path of travel of the boat. Practically speaking, this was not possible. Instead, the radar gun would be stationed on the bank of the river, resulting in a small angle between its line of sight and the path of the travel of the boat. To keep this angle, and the associated error, a small as possible, it was necessary to lock the radar gun on the target when it was far away.

Second, and related to this, the degree to which the commercial operators were maintaining a constant speed is unknown. Therefore, the speed of the boat as it passed the instrumentation may have been appreciably different from the speed measured while the boat was approaching.

4.3.5 Data Acquisition

Two laptops were used to collect the data discussed above. In the case of the ADV, data were collected via the serial port using a DOS-based application supplied with the instrument.

In the cases of the OBS-3 and the wave gages, analog voltage data were collected via a PCMCIA National Instruments data acquisition card (model # DAQ-1200). Management of the acquisition was performed with National Instruments Labview software.

4.3.6 Miscellaneous

At each location where data were taken, attempts were made to measure the discharge in the channel. A prerequisite for this was the ability to wade the entire channel. For most sites, this was possible.

The velocity measurements required for the discharge calculation were made with a Marsh-McBirney Flo-Mate 2000. The accuracy of this instrument is given by ± 2% of the reading ± the zero stability of 0.015 m s^{-1}. Standard surveying methods were used, whereby, if the depth of the water was less than 0.91 m, a single measurement was made at six tenths of the water depth. If the water depth was greater than 0.91 m, measurements were made at both two tenths and eight tenths the water depth and the two measurements were then averaged. The depth-averaged velocity values were then integrated across the width of the channel, using an adaptive recursive Simpson's rule.

Chapter 5

Experimental Procedures and Results

In this chapter, the general experimental procedures are discussed and the obtained data for each site are presented.

5.1 Experimental Design

Broadly speaking, two different types of experiments were conducted. The first type of experiment involved spanning a number of wave gages between the sailing line of a boat and one of the banks of the river. In addition, the OBS-3 was placed very close to (within 25 cm of) the bank and slightly below the water surface. This is shown in Fig. 5.1.

To make the obtained wave data meaningful, it was necessary to determine the distance from the sailing line to the bank. This was done in a variety of ways, depending upon the site. In most cases, a pair of guide buoys, weighted with cinder blocks, would be placed at the desired location. This was a very accurate method, as the precise distance could be measured with a 100 m tape measure. In the case of Site 1, the river was too deep and swift at its center to allow for this. In this case, the width of the river was estimated from GPS measurements and aerial photographs, and a visual estimate of the sailing line (e.g. 1/2 way across, 1/3 way across, etc.) was made for each trial. Finally, in the case of Site 6, Wells Bridge is supported by piers that are 15.25 m apart. By noting which pair of piers the boat passed through, a reasonably accurate estimate of sailing line to bank distance was

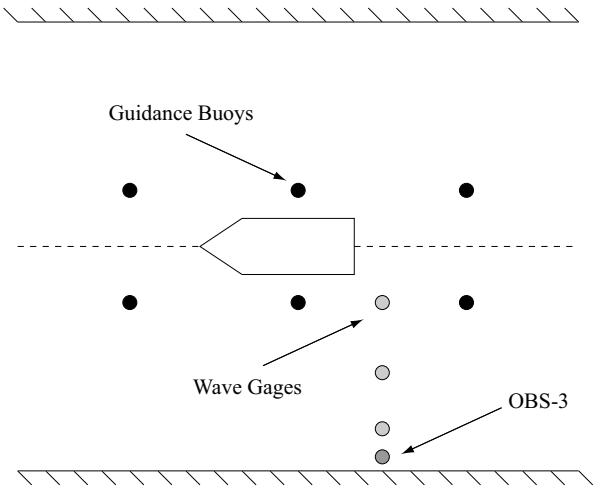

Figure 5.1: Planview of general experimental configuration of wave gages and OBS-3.

made.

The second type of experiment involved making measurements of near-bed induced velocity and suspended sediment concentration. In this case, in addition to having a wave gage adjacent to the river bank, the ADV and the OBS-3 were positioned on the river bed, underneath the sailing line of the boats. This is shown in Fig. 5.2.

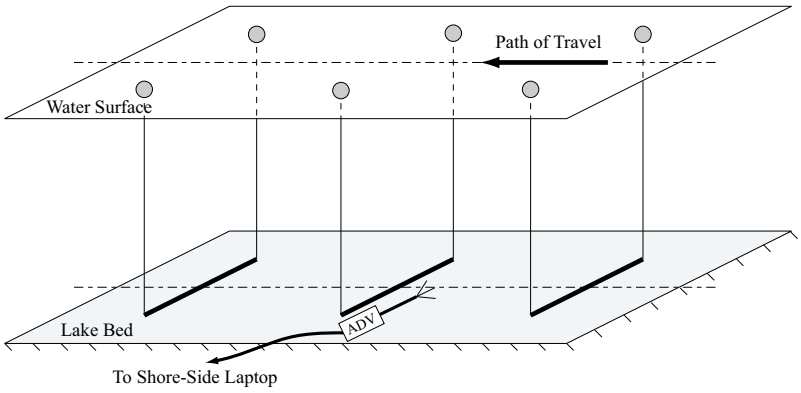

Figure 5.2: Experimental schematic of ADV and OBS-3 (not shown) location.

Regarding experimental procedure, the ideal situation would have allowed for a series of controlled experiments with all of the boats. By systematically

varying parameters such as boat speed, passenger loading, water depth, and distance from shore, a comprehensive picture of the wake characteristics could be built up, as was done by Maynord (2001).

To a limited extent, this was possible with the *FG16* and *FG18* boats, as they were at the disposal of the authors. At the locations where these boats were studied, numerous runs were conducted at a wide range of speeds. Unfortunately, similar variation was not possible with the boats belonging to the commercial operator. Instead, the authors were limited to making uncontrolled measurements of the operator's daily runs, with the result that the data for these boats do not span a very broad range.

Regardless, an individual run would commence when an approaching boat was roughly 100 m from the test site. At this point, the radar gun would be used to ascertain the speed of the boat and the data acquisition would begin. As the boat passed directly by the test site, photographs would be taken, allowing for passenger counts. Data were typically acquired for 2 to 3 minutes after passage of the boat, until the observed fluctuations in the wave gage and OBS-3 output had subsided.

5.2 Data Analysis

Typical output from the near-bank wave gage and OBS-3 are shown in Fig. 5.3. Prior to the boat's arrival, the water level is essentially quiescent and the OBS-3 is reading the background turbidity (due to the glacial silt load of river). The arrival of the boat is manifested in the form of a train of waves, typically consisting of 10 to 20 individual waves. At the same time, the OBS-3 registers a rapid increase in suspended sediment concentration (SSC), followed by a slow decrease. For the example shown, SSC levels remained elevated for several minutes beyond passage of the boat.

As discussed in Chapter 4, in order to relate the output of the OBS-3 to SSC, it was necessary to perform a calibration using a site-specific sediment sample. In all cases, the relationship was extremely linear, as illustrated by the sample shown in Fig. 5.4.

For each sediment sample, therefore, the following linear equation was assumed to hold:

$$SSC = mV + b,$$

where SSC is in grams per liter, V is the voltage output of the OBS-3, and m and b are constants. The best-fit calibration results are summarized in

Table 5.1. Note that Site 1 has a significantly different calibration constant (m) than the other sites. This difference, which is readily explained, is due to the sandy nature of the bank at Site 1. This difference was also evident in Fig. 4.14. The OBS-3 essentially measures the turbidity of the water. A suspension of fine-grained sediments, with their high surface area-to-volume ratio, can attain high values of turbidity at relatively low concentrations. Coarser sediments, on the other hand, require fairly high concentrations to achieve the same turbidity values.

Site	m	b
1	7.56	1.25
2	1.69	0.44
3	0.85	0.15
4	1.04	0.22
5	1.53	0.31

Table 5.1: Calibration constants for the OBS-3.

To relate the output of the wave gages to water surface elevation was a much more straightforward matter, as the calibration is linear, stable and independent of location. Regardless, the gages were re-calibrated at the beginning of each day.

In terms of data analysis, there are numerous quantities of interest, including maximum wave height, average wave height in a train, number of waves in a train, total wave energy in a train, and so forth. Additionally, the maximum observed SSC is of interest as it is an indicator of the impact on the banks. Computation of the wave statistics involves some measure of judgement. For example, returning to Fig. 5.3, it is not immediately obvious when the wave train 'ends'. Additionally, it is not obvious what exactly constitutes a wave in the first place.

As illustrated in Fig. 5.5, a wave record can be analyzed in order to identify the 'crests'. Once this is done, the amount of time between adjacent crests is taken to be the period of an individual wave and the vertical distance between a crest and the following trough is taken to be the height of an individual wave.

To prevent background noise in the data acquisition system and small ripples on the water surface from being counted as boat-associated waves, several steps were taken. First, the data was put through a lowpass filter,

with a cutoff frequency of 1.5 Hz. Second, taking into account that the resolution of the wave gages was $\pm$ 1 cm, all identified 'waves' with wave heights less than this were discarded.

In order to identify the 'end' of a wave train, no consistent method exists in the literature. For example, one could truncate a wave record upon observation of a wave whose amplitude fell below a certain value. The problem with this approach is that wave trains often have 'beats' in them where successive wave heights diminish in amplitude and then grow again. Such a simple truncation would therefore overlook potentially significant amounts of boat-related wave energy.

The following procedure was developed for and proved to be a consistent measure for the present study:

- Segment the wave record into n individual waves ($H_1,\ H_2, \ldots,\ H_i, \ldots,\ H_{n-1},\ H_n$), as discussed above.
- Identify the height $H_{\max}$ and the index $i_{\max}$ of the largest wave in the record.
- For all subsequent waves ($i > i_{\max}$), compute the ratio

$$R \equiv \frac{\sum_{j=i_{\max}}^{i} H_j}{(i - i_{\max}) H_{\max}}. \tag{5.1}$$

- When three successive waves yield $R < 0.5$, terminate the wave record.

As an example, recall the sample wave record given in Fig. 5.3. Upon running this procedure, a total of 18 waves are identified, the fourth of which has the maximum amplitude. Fig. 5.6 plots the successive wave heights in the record, as well as the ratio R. Using the adopted criterion, the wave record is truncated after the eleventh wave.

Once the waves, and their respective heights and periods, have been identified and validated, basic statistics, such as maximum and mean values, along with standard deviations, are easily calculated. Also, the energy of the wave train, per unit meter of bank, is given by summing up the energies in the individual waves

$$E_T = \frac{\rho g}{8} \sum_{j=1}^{n} H_j^2 \lambda_j,$$

where the wavelength of an individual wave, λ_j, is calculated from the dispersion relationship and from the period, T_j, of that wave.

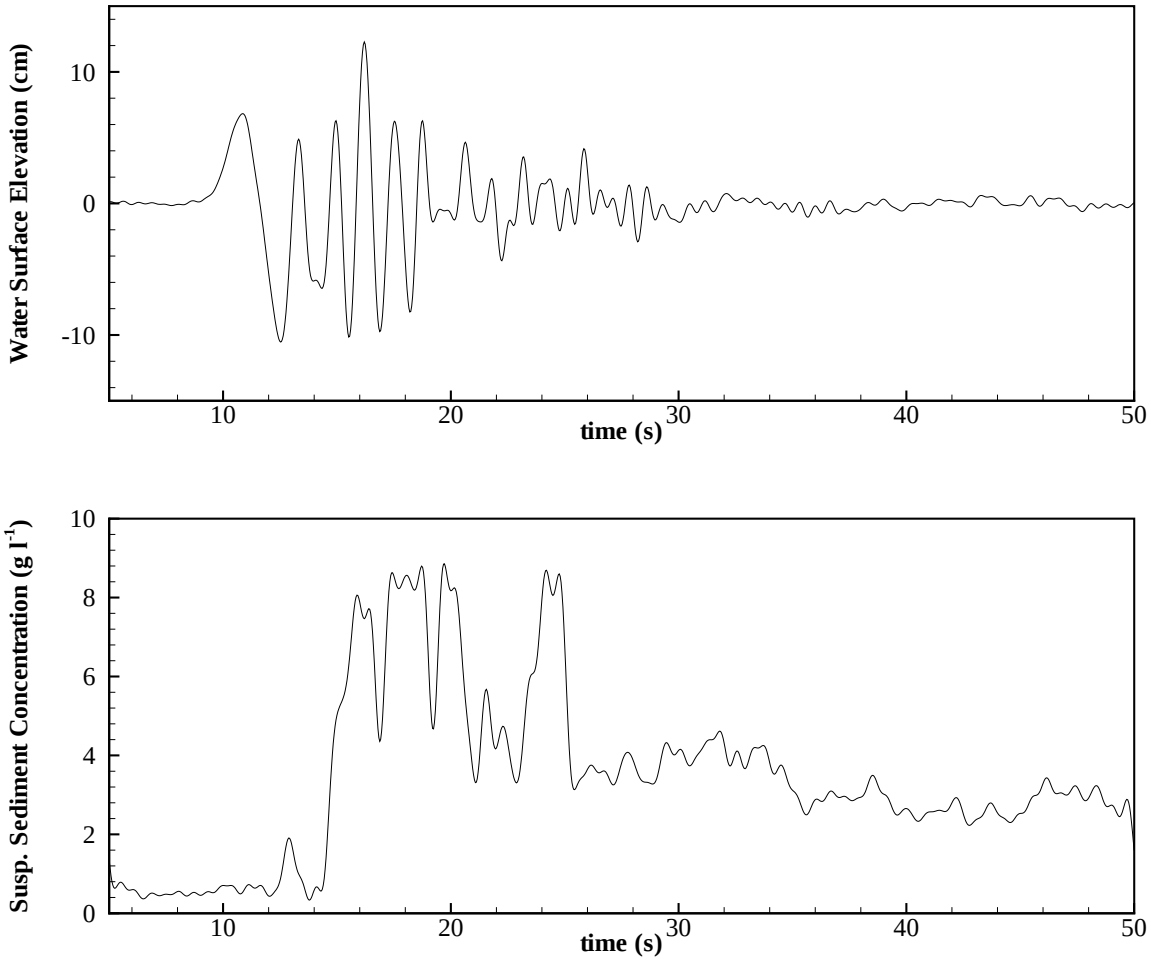

Figure 5.3: Typical output from wave gage and near-bank OBS-3.

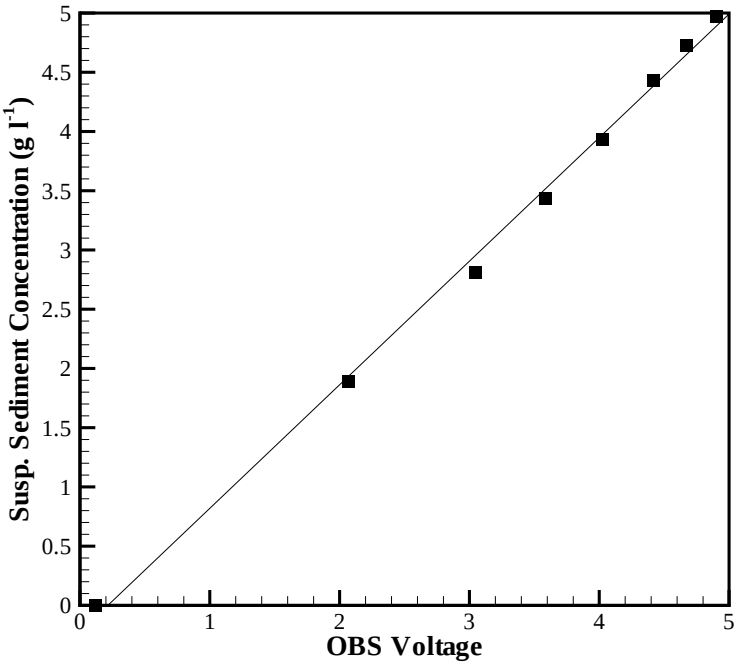

Figure 5.4: OBS-3 calibration data and straight-line fit for Site 4.

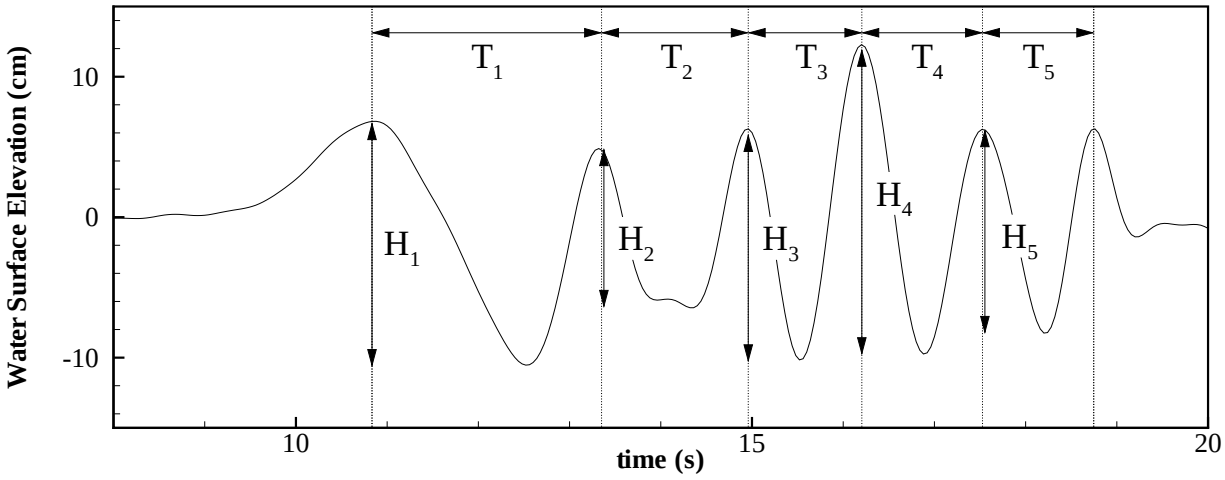

Figure 5.5: Portion of typical wave gage record, illustrating segmentation of record and identification of wave heights and periods.

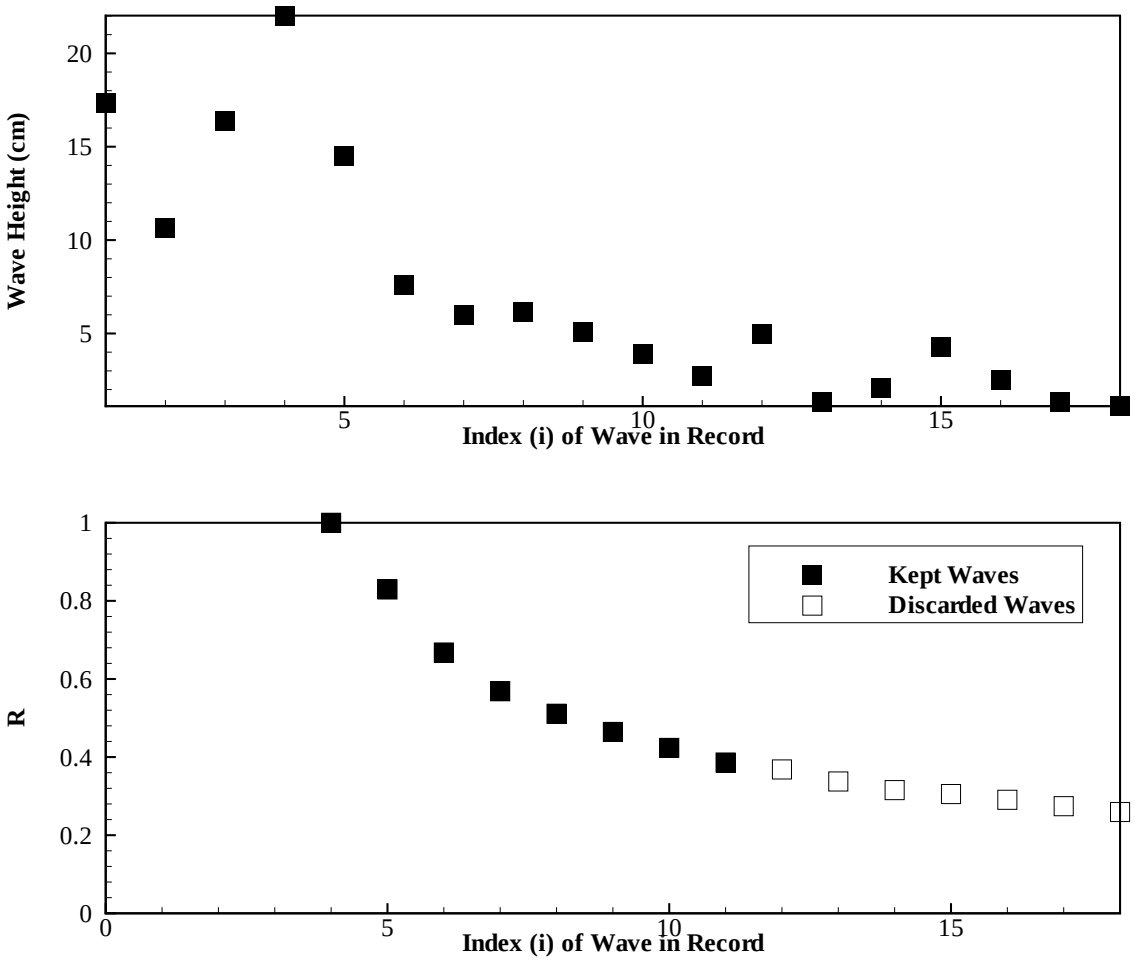

Figure 5.6: Plot of successive wave heights in the sample wave record shown in Fig. 5.3. Also shown is the ratio R, defined in (5.1), used in determining truncation point of wave record.

5.3 Results

In this section, a site-by-site summary of the experimental parameters, relevant wave characteristics, and observed maximum suspended sediment concentration will be given. Note the following:

- In the following tables of results, boat 'direction' refers to travel upstream (US) or downstream (DS).
- The passenger counts represent a 'conservative' estimate, i.e. a lower bound. Due to the fact that the photographs were taken from the same vertical elevation (on the bank) as the passing boats, it was frequently difficult to discern whether or not any passengers on the 'far' side of the boat were hidden from view.
- Total mass refers to the sum of boat, engine, and passenger masses. The average mass of a male over the age of 20 is 82 kg and that of a female over the age of 20 is 68 kg, according to the Centers for Disease Control and Prevention. The authors have therefore assumed an equal distribution of males and females so that an average passenger mass of 75 kg is used in estimating total mass. No attempt was made to estimate the additional mass of fuel and accessories.
- The OBS-3 was factory calibrated to sense between 0 and 500 FTUs (Formazin Turbidity Units). In numerous trials, enough sediment was dislodged that the sensor 'pegged out' at its maximum reading. In those trials, all that can be said is that the maximum SSC exceeded the range of the sensor.

5.3.1 Site 1

At this site, a single wave gage and the OBS-3 were set up adjacent to the right bank. The water depth at the location of the gage was 0.36 m. A total of eleven trials were performed. In all cases, the boat was judged to be approximately in the middle of the channel, yielding a distance from sailing line to bank of approximately $x = 35$ m. The water depth at the sailing line was unknown.

Trial	Boat	Passenger Loading	Total Mass (kg)	Direction	V_b (mph)	x (m)	# of Waves	H_{max} (cm)	H_{mean} (cm)	T_{mean} (s)	E_T (J m^{-1})	SSC_{max} (g l^{-1})
1	*COM32*	20	2885	US	14.0	35	19	25.61	10.89	1.58	5440	24.5
2	*COM20*	8	1330	US	19.0	35	13	14.57	5.98	1.18	510	8.0
3	*COM20*	8	1330	DS	22.0	35	44	15.3	5.03	0.67	350	20.6
4	*COM32*	20	2885	DS	26.0	35	14	15.43	6.40	1.16	740	>40.0
5	*COM32*	19	2810	US	18.0	35	15	25.92	12.33	1.59	2550	>40.0
6	*COM32*	19	2810	DS	24.0	35	9	21.44	10.05	1.36	1080	>40.0
7	*COM32*	12	2285	US	21.0	35	16	18.75	9.8	1.32	1400	>40.0
8	*COM32*	12	2285	DS	26.0	35	11	14.86	6.85	1.04	580	32.2
9	*COM32*	18	2735	DS	25.1	35	19	18.18	8.63	1.10	720	>40.0
10	*COM32*	18	2735	US	18.0	35	18	23.21	9.8	1.20	1180	32.1
11	*COM32*	18	2735	DS	23.0	35	17	21.07	9.57	1.10	680	37.5

Table 5.2: Summary of data for Site 1.

5.3.2 Site 2

At this site, a single wave gage and the OBS-3 were set up adjacent to the right bank. In this case, the depth of water at the location of the gage was approximately 1.0 m. A single buoy was used to guide the boats along a sailing line approximately 20 m from the bank. The water depth at the sailing line was roughly measured to be 1.5 m. A total of 11 trials were performed.

Trial	Boat	Passenger Loading	Total Mass (kg)	Direction	V_b (mph)	x (m)	# of Waves	H_{max} (cm)	H_{mean} (cm)	T_{mean} (s)	E_T (J m^{-1})	SSC_{max} (g l^{-1})
1	*COM24*	12	1890	DS	18.3	20	10	22.01	10.60	1.34	740	>8.9
2	*COM32*	28	3490	DS	20.8	20	10	23.41	9.65	1.19	1050	>8.9
3	*COM32*	18	2740	DS	21.5	20	6	18.79	8.10	1.27	660	>8.9
4	*FG16*	1	290	DS	23.5	20	19	6.45	3.02	1.19	60	3.04
5	*FG16*	1	290	US	18.5	20	17	5.24	2.78	1.29	60	2.65
6	*FG16*	1	290	DS	17.5	20	15	8.77	4.22	1.25	110	2.63
7	*FG16*	1	290	US	14.0	20	15	6.43	3.52	1.56	100	3.25
8	*FG16*	1	290	DS	14.5	20	17	7.86	4.39	1.10	100	3.56
9	*FG16*	1	290	US	12.2	20	14	5.86	3.66	1.47	100	4.41
10	*FG16*	1	290	DS	12.2	20	20	8.94	4.28	1.02	110	5.62
11	*FG16*	1	290	US	9.0	20	18	5.91	3.30	1.44	110	4.97

Table 5.3: Summary of data for Site 2.

5.3.3 Site 3

At this location, three wave gages spanned the distance from the middle of the channel to the right bank. Buoy pairs were used to guide the boat along the desired path of travel. The sailing line was 39.3 m from the wave gage closest to the bank. As wave heights at the bank were of primary interest in this study, the presentation of results will be limited to observations at the banks. The water depth at this location was 0.69 m. The water depth at the sailing line was 0.81 m. A total of 9 trials were performed, but three had to be discarded due to difficulties with the instrumentation.

Trial	Boat	Passenger Loading	Total Mass (kg)	Direction	V_b (mph)	x (m)	# of Waves	H_{max} (cm)	H_{mean} (cm)	T_{mean} (s)	E_T (J m^{-1})	SSC_{max} (g l^{-1})
1	*COM20*	11	1560	US	19.4	39.3	28	13.99	4.03	0.55	200	1.55
2	*COM32*	16	2585	DS	22.0	39.3	10	22.98	8.75	0.85	690	1.41
3	*COM32*	18	2740	DS	23.7	39.3	16	17.95	8.5	0.67	380	4.74
4	*COM24*	11	1810	DS	20.5	39.3	25	13.14	5.54	0.72	180	1.99
5	*COM20*	10	1480	US	17.0	39.3	8	11.83	5.24	0.61	120	1.01
6	*COM32*	22	3040	DS	17.5	39.3	12	20.17	6.81	0.68	250	2.04

Table 5.4: Summary of data for Site 3.

5.3.4 Site 4

For these trials, a single wave gage was set up adjacent to the right bank of the river. The wave gage was in 0.3 m of water and was at a distance of 6.0 m from the sailing line. The OBS-3 was set up on the river bottom, underneath the passing boats, rather than adjacent to the bank. A total of 24 trials were performed and the water depth at the sailing line was 1.04 m. The general parameters and wake characteristics are summarized in Table 5.5. Note that, for several trials, the boat speed was below the lower limit of the radar gun, therefore precluding a measurement of speed for those trials. Also, note that no data are available for Trial 14, as, according to the analysis procedure outlined in §5.2, no waves were detected.

Trial	Boat	Passenger Loading	Total Mass (kg)	Direction	V_b (mph)	x (m)	# of Waves	H_{max} (cm)	H_{mean} (cm)	T_{mean} (s)	E_T (J m^{-1})
1	*COM32*	16	2590	US	6.0	6.0	8	23.56	8.74	1.53	2840
2	*COM32*	16	2590	DS	< 5.0	6.0	13	9.27	3.22	0.94	30
3	*COM32*	22	3040	US	< 5.0	6.0	6	11.72	5.23	1.11	80
4	*COM32*	22	3040	DS	< 5.0	6.0	16	4.48	2.09	0.88	10
5	*COM24*	16	2190	US	< 5.0	6.0	9	9.99	4.47	1.04	60
6	*COM24*	16	2190	DS	< 5.0	6.0	14	5.45	2.37	0.81	10
7	*COM32*	22	3040	US	< 5.0	6.0	8	12.98	5.40	0.94	90
8	*COM32*	22	3040	DS	< 5.0	6.0	13	4.13	2.12	0.90	10
9	*COM32*	23	3110	US	19.6	6.0	6	30.70	12.53	1.37	1000
10	*COM32*	23	3110	DS	19.4	6.0	6	29.48	13.1	1.37	1000
11	*COM24*	8	1590	US	20.4	6.0	7	21.92	7.84	1.05	380
12	*COM24*	8	1590	DS	15.0	6.0	7	28.38	12.03	1.11	900
13	*FG16*	1	285	US	3.0	6.0	9	2.05	1.26	0.86	0
14	*FG16*	1	285	DS	3.0	6.0	–	–	–	–	–
15	*FG16*	1	285	US	4.7	6.0	5	9.95	3.50	1.06	30
16	*FG16*	1	285	DS	4.8	6.0	11	6.98	3.06	0.91	20
17	*FG16*	1	285	US	10.1	6.0	7	19.35	8.31	1.29	260
18	*FG16*	1	285	DS	9.7	6.0	9	18.22	8.23	1.29	330
19	*FG16*	1	285	US	7.7	6.0	8	19.36	8.00	1.13	320
20	*FG16*	1	285	DS	8.4	6.0	10	18.27	7.99	1.12	400

Table 5.5: Summary of data for Site 4.

Trial	Boat	Passenger Loading	Total Mass (kg)	Direction	V_b (mph)	x (m)	# of Waves	H_{max} (cm)	H_{mean} (cm)	T_{mean} (s)	E_T (J m^{-1})
21	*FG16*	1	285	US	11.9	6.0	7	18.73	7.52	1.38	240
22	*FG16*	1	285	DS	12.2	6.0	10	15.98	6.21	1.43	280
23	*FG16*	1	285	US	15.5	6.0	8	14.30	6.30	1.30	150
24	*FG16*	1	285	DS	15.3	6.0	9	14.43	5.74	1.32	160

Table 5.5: (continued)

This site was unique in that it allowed for the limited measurement of the flow induced underneath the passing boat. The ADV was positioned such that its measurement volume was 10 cm above the river bottom and directly beneath the sailing line of the boats. The goal of these measurements was to assess the potential for the boats to 'scour' the river bottom. As mentioned, the OBS-3 was also placed underneath the sailing line with the result that the SSC measurements in this case pertain to bottom scour and not bank impacts.

A typical record of the streamwise induced velocity recorded by the ADV is shown in Fig. 5.7. The initial positive velocity is due to the water being pushed ahead by the displacement of the hull. The stronger negative velocity that follows is due to the prop wash of the boat.

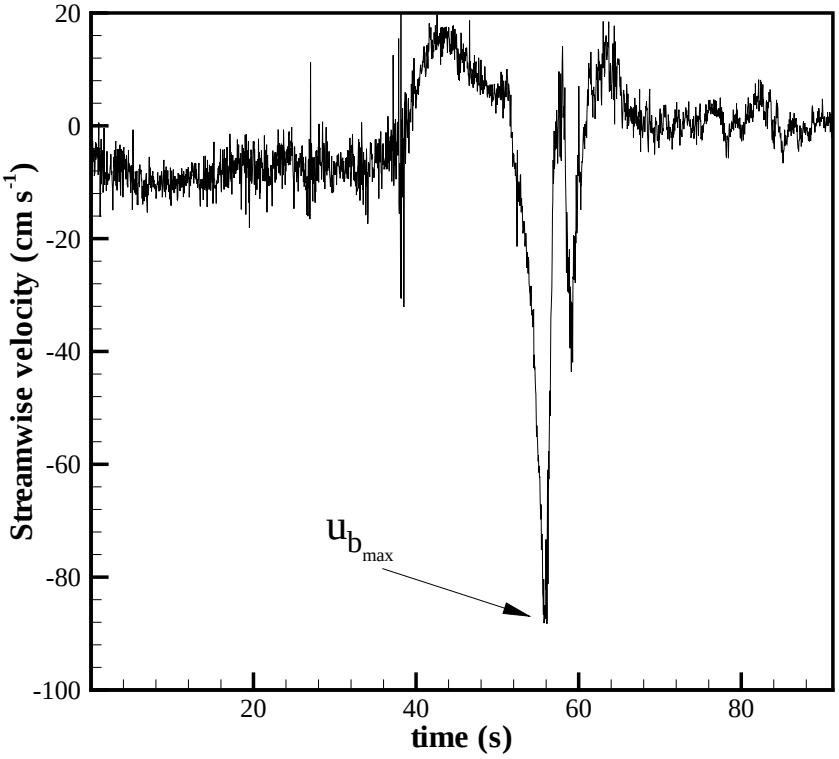

Figure 5.7: Typical ADV record of streamwise velocity showing initial forward 'push' due to hull displacement effects and subsequent backward 'push' due to prop-wash effects. Note the definition of $u_{b_{\max}}$, the maximum observed near-bed velocity.

For all trials where the ADV was so utilized, the maximum observed near-bed velocity was determined, as well as the maximum near-bed SSC. These results are tabulated in Table 5.6.

Trial	$u_{b_{\max}}$ (cm s^{-1})	SSC_{max} (g l^{-1})
3	-	>5.42
4	-	2.97
5	-	>5.42
6	-	>5.42
7	79.31	>5.42
8	40.55	3.93
9	26.06	>5.42
10	20.08	>5.42
11	14.69	>5.42
12	34.78	>5.42
13	13.79	5.13
14	12.99	-
15	22.72	4.36
16	20.08	1.48
17	11.43	3.40
18	16.26	3.74
19	17.14	>5.42
20	16.43	3.86
21	13.67	2.69
22	13.74	1.56
23	18.49	2.16
24	9.02	0.47

Table 5.6: Measurements of maximum observed near-bed velocity and near-bed SSC.

5.3.5 Site 5

At this location, three wave gages were spanned between the sailing line and the left bank. The OBS-3 was positioned adjacent to the left bank. Again, as emphasis was on near-bank conditions, reported wave results will be limited to the wave gage closest to the bank. This gage was in 1.1 m of water and was a distance of 20.2 m from the sailing line. The water depth at the sailing line was 0.45 m.

Trial	Boat	Passenger Loading	Total Mass (kg)	Direction	V_b (mph)	x (m)	# of Waves	H_{max} (cm)	H_{mean} (cm)	T_{mean} (s)	E_T (J m^{-1})	SSC_{max} (g l^{-1})
1	*FG18*	1	340	US	24.5	20.2	6	6.92	3.01	1.61	50	1.00
2	*FG18*	1	340	DS	27.5	20.2	17	8.17	3.85	1.00	80	1.33
3	*FG18*	1	340	US	21.0	20.2	7	7.70	3.58	1.11	50	1.64
4	*FG18*	1	340	DS	23.0	20.2	16	9.24	4.16	0.87	80	1.69
5	*FG18*	1	340	US	17.1	20.2	9	6.32	2.97	0.84	30	1.04
6	*FG18*	1	340	DS	17.4	20.2	12	10.45	4.05	0.74	30	1.88
7	*FG18*	1	340	US	15.1	20.2	9	7.86	3.21	1.21	70	2.17
8	*FG18*	1	340	DS	18.1	20.2	19	9.89	4.35	0.97	160	2.17
9	*FG18*	1	340	US	15.1	20.2	8	7.33	2.88	0.93	30	2.47
10	*FG18*	1	340	DS	15.0	20.2	5	10.68	4.69	1.42	250	3.09
11	*FG18*	1	340	US	11.3	20.2	6	10.82	3.93	1.26	200	2.66
12	*FG18*	1	340	DS	12.7	20.2	5	9.01	3.64	0.99	40	2.38

Table 5.7: Summary of data for Site 5.

5.3.6 Site 6

For these trials, a single wave gage and the OBS-3 were set up immediately adjacent to the left bank of the river. The wave gage was in approximately 1.0 m of water. A total of four trials were performed. For all trials, the water depth at the sailing line was unknown.

Trial	Boat	Passenger Loading	Total Weight (kg)	Direction	Speed (mph)	x (m)	No. of Waves	H_{max} (cm)	H_{mean} (cm)	T_{mean} (s)	Energy (J m^{-1})
1	*COM32*	17	2660	DS	28.5	38.0	13	19.82	10.19	1.55	860
2	*COM32*	17	2660	US	17.0	53.0	19	16.57	8.16	2.12	1620
3	*COM32*	14	2440	DS	24.0	53.0	20	17.29	8.11	1.59	1050
4	*COM32*	14	2440	US	19.5	53.0	23	17.45	7.64	1.70	1620

Table 5.8: Summary of data for Site 6.

Chapter 6

Analysis & Discussion

In this chapter, a discussion of some of the apparent trends in the data is offered. Additionally, some calculations are presented in an effort to weigh the potential impacts of boat wakes on the Chilkat River relative to those of the base stream flow.

6.1 Discussion of Results

As mentioned previously in Chapter 5, the trials with the commercial boats were limited in number, with the consequence that the data are similarly limited. Moreover, the data that do exist do not vary the relevant parameters as systematically as is desired. Nonetheless, some useful trends emerge upon consideration of the raw, dimensional data and the scaled, non-dimensional data.

6.1.1 Observed Trends

For example, it is of interest to know how observed values of H_{max} vary with boat size. Table 6.1 summarizes, on a site by site basis, the ensemble-averaged value of H_{max} ($\overline{H_{max}}$) observed for each boat. Also given are the numbers of trials available for computing the average. Note that, in the case of Site 4, the non-planing runs of the commercial boats were not used in computing the average. Also note that the averages cited for the *FG16* and *FG18* boats are over-estimates, compared to those of the commercial boats. This is because, in all cases, the commercial boats were operating

'on-step', which yields relatively small wakes. The runs for the ADFG boats intentionally spanned a wide range of speeds, including semi-planing and displacement speeds, which, for a give boat, create relatively large wakes. Regardless, at any given site, the data indicate that wake height roughly increases with boat size.

Site	Boat	# Trials	$\overline{H_{max}}$ (cm)
1	*COM20*	2	14.9
	COM32	9	20.5
2	*FG16*	8	6.9
	COM24	1	22.0
	COM32	2	21.1
3	*COM20*	2	12.9
	COM24	1	13.1
	COM32	3	20.4
4	*FG16*	12	13.14
	COM24	2	25.1
	COM32	2	30.1
5	*FG18*	12	8.7
6	*COM32*	4	17.8

Table 6.1: Ensemble-averaged values of H_{max}, sorted by boat and by site.

Recall, of course, that sailing line distances were different at the different sites. If this is neglected for the moment and *all* runs by a particular boat are used in obtaining an 'overall' average value of H_{max}, the results, shown in Table 6.2, again indicate a moderate correlation between boat size and maximum wake height.

Boat	$\overline{H_{max}}$ (cm)
FG16	10.6
FG18	8.7
COM20	13.9
COM24	21.3
COM32	21.0

Table 6.2: Ensemble-averaged values (using *all* trials) of H_{max}, sorted by boat.

A second question of significant interest is how the near-bank 'impact' varies with the loading on the bank (i.e. H_{max}). Other studies (Nanson *et al.*, 1994; Dorova and Moore, 1997) have shown that impact, whether measured by swash load or by erosion pins, tends to increase with increasing wave heights. The same trend is evident in the current study. For example, if the controlled runs with *FG18* at Site 5 are considered, there is an evident increase in SSC_{max} with increasing H_{max}, as shown in Fig. 6.1.

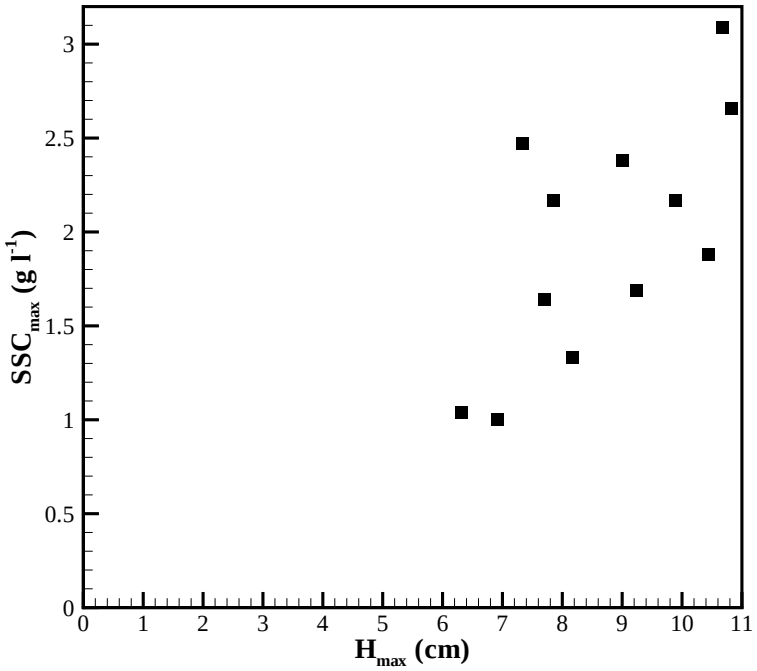

Figure 6.1: Maximum observed values of near-bank SSC as a function of H_{max} for Site 5.

Finally, it is worth discussing Site 4 in particular, in light of the decision, referred to in Chapter 4, by ADFG to restrict commercial traffic there to 'slow-no wake' operation. Table 6.3 summarizes the ensemble-averaged values of maximum observed near-bed velocity, sorted by boat and mode of operation. First of all, observe that there is again a dependence upon boat size, with *FG16* registering a smaller signal at the river bed than the commercial boats.

More interesting is the observation that the commercial boats travelling at seemingly slow speeds register a larger signal than those travelling at

Boat	# Trials	Notes	$\overline{u_{b_{max}}}$ cm s^{-1}
COM24	2	planing	24.7
COM32	2	planing	23.1
COM32	2	'slow-no wake'	59.9
FG16	12	all speeds included	15.5

Table 6.3: Ensemble-averaged values of $u_{b_{max}}$.

high speeds. This is the precise result found by Beachler (2002) and Yousef *et al.* (1978). Those studies showed that boats travelling near the 'critical' speed of $(gh)^{1/2}$ induced the largest near-bed velocity while those travelling much slower or much faster than $(gh)^{1/2}$ had less impact on the bed. Recalling the definition of the depth-based Froude number from Chapter 3 ($Fr_d \equiv V_b/(gh)^{1/2}$), this amounts to boats operating at $Fr_d \ll 1$ or $Fr_d \gg 1$ minimizing bottom impacts and boats operating at $Fr_d \sim 1$ maximizing impacts.

For Site 4, where the depth was 1.04 m, a boat travelling at 20 mph has a depth-based Froude number of 2.8. A boat travelling at 5 mph, on the other hand, has a depth-based Froude number of 0.7, which is less optimal. To distance Fr_d from the critical value in the case of 'slow-no wake' operation, therefore, boat speeds should be brought down further, with the boat operating at its so-called engagement speed (just in gear).

Of course, the question of bottom impacts must be considered in tandem with the question of bank impacts. Table 6.4 summarizes the ensemble-averaged values of H_{max} and it is clear that planing operation generates significantly larger wakes at the banks than 'slow-no wake' operation.

Boat	# Trials	Notes	$\overline{H_{max}}$ cm
COM24	2	'slow-no wake'	7.7
COM24	2	planing	25.2
COM32	6	'slow-no wake'	11.0
COM32	2	planing	30.1

Table 6.4: Ensemble-averaged values of H_{max}.

6.1.2 Scaling of Results

While the results of the present study are useful in their current, dimensional form, it is more useful to consider them in non-dimensional format. This is because, if scaled appropriately, trends common to all of the boats studied should appear. The difficulties in applying this reasoning to the present study are two-fold. First, the data are rather limited. Second, the multitude of length scales present in the problem (water depth, sailing line-to-bank distance, boat length) raises a number of scaling possibilities.

As discussed in Chapter 3, maximum wave heights are expected to depend upon the depth- and length-based Froude numbers Fr_d and Fr_l. They are also expected to depend upon the distance from sailing line to gage. After considering the numerous possibilities, it turns out that both H_{max} and x scale best with the boat length L. The dimensional results of Chapter 5 are therefore recast in Table 6.5, grouped first by boat and then by site. The trial numbers are the same as those given in the previous chapter.

Site	Trial	Fr_d	Fr_l	x/L	H_{max}/L
FG16					
2	4	2.74	1.52	3.93	0.0133
	5	2.16	1.20	3.93	0.0108
	6	2.04	1.14	3.93	0.0181
	7	1.63	0.91	3.93	0.0133
	8	1.69	0.94	3.93	0.0162
	9	1.42	0.79	3.93	0.0121
	10	1.42	0.79	3.93	0.0185
	11	1.05	0.58	3.93	0.0122
4	13	0.42	0.19	1.24	0.0042
	14	0.42	0.19	1.24	0.0000
	15	0.66	0.30	1.24	0.0206
	16	0.67	0.31	1.24	0.0144
	17	1.41	0.66	1.24	0.0400
	18	1.36	0.63	1.24	0.0376
	19	1.08	0.50	1.24	0.0400
	20	1.18	0.54	1.24	0.0377
	21	1.67	0.77	1.24	0.0387
	22	1.71	0.79	1.24	0.0330
	23	2.17	1.01	1.24	0.0295

Table 6.5: Scaled wave data for all sites and boats.

Site	Trial	Fr_d	Fr_l	x/L	H_{max}/L
	24	2.14	0.99	1.24	0.0298
FG18					
5	1	5.21	1.48	3.61	0.0124
	2	5.85	1.66	3.61	0.0146
	3	4.47	1.27	3.61	0.0138
	4	4.89	1.39	3.61	0.0165
	5	3.64	1.03	3.61	0.0113
	6	3.70	1.05	3.61	0.0187
	7	3.21	0.91	3.61	0.0140
	8	3.85	1.09	3.61	0.0177
	9	3.21	0.91	3.61	0.0131
	10	3.19	0.90	3.61	0.0191
	11	2.40	0.68	3.61	0.0193
	12	2.70	0.77	3.61	0.0161
COM20					
1	2	-	1.10	5.74	0.0239
	3	-	1.27	5.74	0.0251
3	1	3.08	1.12	6.44	0.0229
	5	2.70	0.98	6.44	0.0194
COM24					
2	1	2.13	0.97	2.60	0.0302
3	4	3.25	1.08	5.38	0.0180
4	11	2.85	1.08	0.82	0.0300
	12	2.10	0.79	0.82	0.0389
COM32					
1	1	-	0.64	3.57	0.0261
	4	-	1.19	3.57	0.0157
	5	-	0.82	3.57	0.0264
	6	-	1.09	3.57	0.0219
	7	-	0.96	3.57	0.0191
	8	-	1.19	3.57	0.0152
	9	-	1.14	3.57	0.0186
	10	-	0.82	3.57	0.0237
	11	-	1.05	3.57	0.0215
2	2	2.42	0.95	1.94	0.0239
	3	2.51	0.98	1.94	0.0192

Table 6.5: Scaled wave data for all sites and boats.

Site	Trial	Fr_d	Fr_l	x/L	H_{max}/L
3	2	3.49	1.00	4.01	0.0234
	3	3.76	1.08	4.01	0.0183
	6	2.78	0.80	4.01	0.0206
4	1	0.84	0.27	0.61	0.0240
	9	2.74	0.89	0.61	0.0313
	10	2.72	0.88	0.61	0.0301
6	1	-	1.30	3.88	0.0202
	2	-	0.78	5.41	0.0169
	3	-	1.09	5.41	0.0176
	4	-	0.89	5.41	0.0178

Table 6.5: Scaled wave data for all sites and boats.

Of greatest interest, from a management point of view, is the ability to predict the maximum wave height that will occur at the bank for a given boat and given sailing line. As illustrated by Fig. 6.2, the correlation between the nondimensional maximum wave height and both Froude numbers is fairly poor, yielding these parameters poor predictors of expected wave heights on the Chilkat. Note also from this figure that the commercial boats operate at speeds and depth that are favorable ($Fr_d > 1$ and $Fr_l > 0.5$) in terms of minimizing wave heights.

Better success is had when the scaled maximum wave height is plotted against the scaled distance from sailing line to shore, as shown in Fig. 6.3. A power-law curve fit is adopted, yielding the following relationship:

$$\frac{H_{max}}{L} = 0.033\left(\frac{x}{L}\right)^{-0.43}. \tag{6.1}$$

The usefulness of (6.1) is that, if it is desired to keep the wave heights at the bank below a certain threshold value (as examples, Dorova and Moore (1997) cite a value of ~ 15 cm and Nanson *et al.* (1994) cite a value of ~ 30 cm), the minimum sailing line-to-bank distance can be estimated for a given size boat. Solving (6.1) for x yields

$$x_{min} = \left(0.033\frac{L^{1.43}}{H_{max}}\right)^{2.33}. \tag{6.2}$$

Representative values of x_{min}, for the boats studied herein, for these two suggested bank wave height criteria are summarized in Table 6.6. Note the strong influence of both boat length and allowable H_{max}.

Boat	H_{max} (cm)	x_{min} (m)
FG16	30	1.1
	15	5.6
FG18	30	1.8
	15	9.1
COM20	30	2.4
	15	12.1
COM24	30	4.4
	15	22.1
COM28	30	7.3
	15	36.7
COM32	30	11.8
	15	59.0

Table 6.6: Minimum sailing line distances needed to keep wave heights below specified H_{max}.

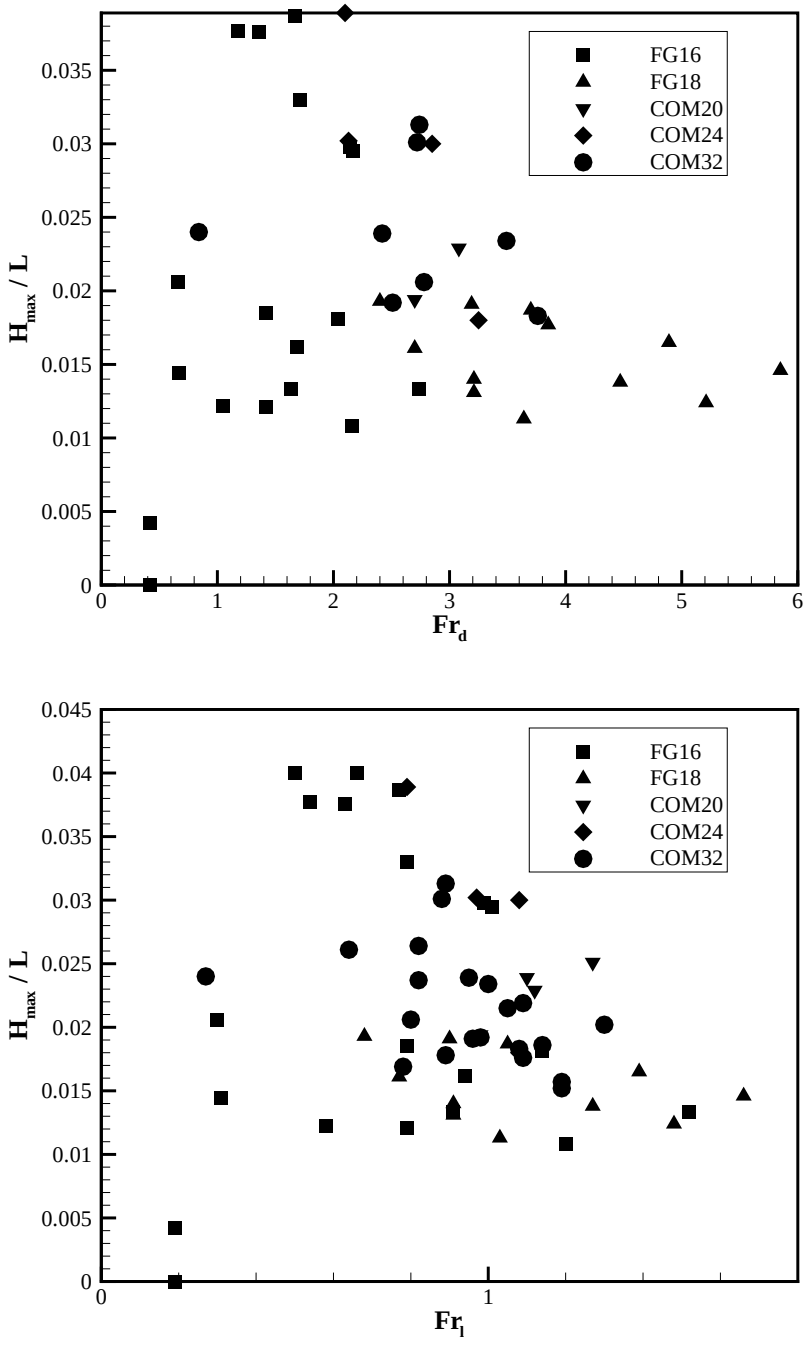

Figure 6.2: Non-dimensional maximum wave heights, as functions of depth- and length-based Froude numbers, for all boats studied.

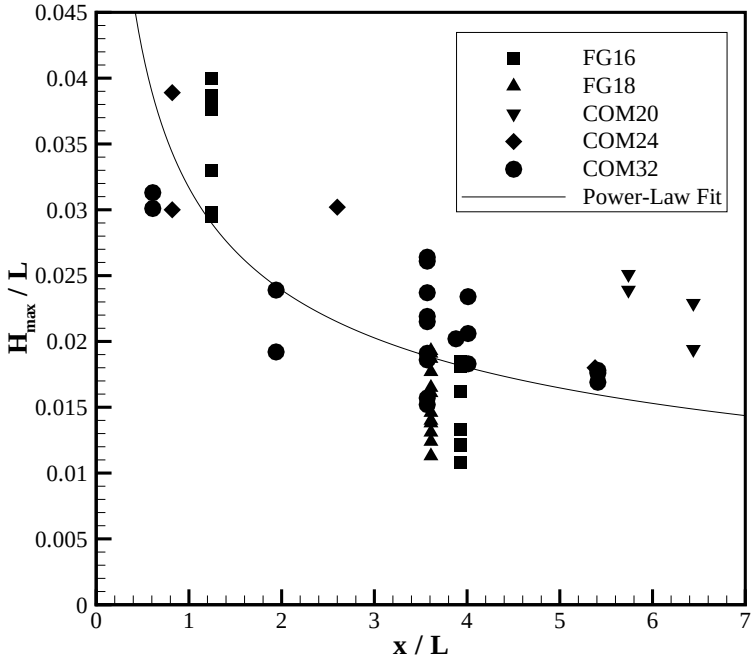

Figure 6.3: Non-dimensional maximum wave heights, as function of non-dimensional distance from sailing line to shore.

6.2 Comparisons with Streamflow

Making a direct comparison between bank impacts associated with boat wakes and those due to streamflow is quite difficult for a number of reasons. First of all, the mechanisms are quite different; streamflow is parallel to the banks and therefore exerts tangential shear stresses on the banks. Wakes, on the other hand, impact the banks nearly perpendicularly. Also, streamflow is an ever-present source of forcing whereas wakes are finite in duration.

Moreover, it is not even clear which quantities are suitable for comparison. One obvious candidate is energy. As previous authors have done, and as is done for the present study in §6.2.1, the amount of wake energy dissipated against the banks can be compared to the amount of streamflow energy dissipated against the banks. However, there are potential flaws with this argument. The hydraulic climate at the banks of a river is frequently quite calm, relative to that in the thalweg, or main channel. Specifically, values of velocity, turbulence intensity, and shear stress are less near the banks. So while it is true that energy is continually being dissipated at the banks, it may be the case that it is occurring at levels low enough to preclude significant impact.

Boat wakes, on the other hand, while limited in duration, may be far more 'intense'. This is evidenced by the OBS-3 records which show a relatively low level of background near-bank turbidity followed by a sharp 'spike' in response to a set of wakes. This raises the question of whether or not total energy should be compared or whether it might be more appropriate to consider power, which is the *rate* of energy dissipation. By way of analogy, consider an electrical circuit. An appliance with a low current draw (and therefore power), but which is on all the time, may end up consuming a large number of kilowatt-hours (energy). Now, consider a second appliance, this one with a very high current draw, but which is used only intermittently. If the energy consumption of the second appliance is lower than the first, but the high current draw blows a fuse, which has had the greater impact?

Another quantity of interest is shear stress. As detailed in, for example, Nielson (1992), when the bed or bank shear stress exceeds some critical value, sediment motion is initiated. This critical value is a strong function of the sediment and bed parameters. The shear stress due to both the streamflow and the boat wakes can therefore be estimated and compared, as detailed below in §6.2.2.

6.2.1 Energy Calculations

First of all, the energies associated with boat waves have already been tabulated in Chapter 5. While these trials were conducted under a wide variety of conditions, it is nonetheless useful to consider the *average* energy, per unit meter of bank, associated with the wave train of a particular boat. As illustrated in Table 6.7 these data do seem to indicate some correlation between boat size and wave energy. Note that no data are available for the *COM30* boat. Using a linear curve fit between boat length and boat energy, therefore, the average energy for that boat is estimated at 900 J m^{-1}.

Boat	# of Trials	E_{mean} (J m^{-1})
FG16	20	150
FG18	12	90
COM20	4	350
COM24	6	380
COM30	-	900
COM32	26	1070

Table 6.7: Mean energy, per unit meter of bank, of the wave trains of the different boats studied.

Combining this information with usage data for the 1999-2001 seasons, it is possible to compute the total boat-wake energy, again per meter of bank length, available for dissipation on the banks. These calculations are summarized in Table 6.8. Note that at some locations, including Sites 1, 4, and 6, each boat trip passes the site twice, once in each direction. Thus, at those sites, the annual totals given in the table should be doubled.

Next, it is necessary to consider the energy of the streamflow itself. For the sake of arriving at some rough numbers, a number of simplifying assumptions will be made. First of all, recall from Fig. 2.5 that there is a strong annual variation in the discharge of the Chilkat River. Flows are highest during a five month period, from May to October. It is reasonable to assume that much of the erosion that is associated with streamflow is therefore confined to this period. Furthermore, it will be assumed that the discharges measured by the authors during the field study are representative of the flows during this period.

The energy dissipated in an open channel flow (see Fig. 6.4) can be estimated as follows. Presuming that a state of uniform flow exists in the reach

Year	Boat	# Trips	Total Energy (J m^{-1})
1999	*COM20*	144	50,400
	COM24	204	77,520
	COM30	191	171,900
			299,800
2000	*COM20*	122	42,700
	COM24	181	68,780
	COM30	180	162,000
	COM32	200	214,000
			487,500
2001	*COM20*	40	14,000
	COM24	97	36,860
	COM30	122	109,800
	COM32	220	235,400
			396,060

Table 6.8: Calculations of annual wake energy generated by the various boats studied.

of interest, the friction slope S_f (of the energy grade line) is equivalent to the bottom slope S_0.

The bottom slope is calculated from the Manning equation,

$$Q = \frac{1}{n} A R_h^{2/3} S_0^{1/2},$$

where Q is discharge, A is cross-sectional area, $R_h \equiv A/\mathcal{P}$ is the hydraulic radius ($\mathcal{P}$ is the wetted perimeter), and n is the Manning parameter. While there is wide variation in n (tabulated values are available in, e.g., Sturm (2001)), a value of 0.025 will be assumed here.

Once $S_0 = S_f$ has been calculated, the head loss h_f in a 1 m length of channel is given by $h_f = S_f \cdot 1$ m. Finally, the perimeter-averaged power (i.e. rate of energy dissipation) per unit meter of bank is given by $P = \gamma h_f Q$, where $\gamma = 9790$ N m^{-3} is the specific weight of water.

Next, it must be noted that this power is the total power dissipated by the full wetted perimeter of the cross-section. Thus, this figure should be multiplied by a factor F (ranging from 0 to 1) which takes into account the fraction of the wetted perimeter that is made up by the banks. This factor can be estimated from the cross-sectional depth surveys. Thus, the power

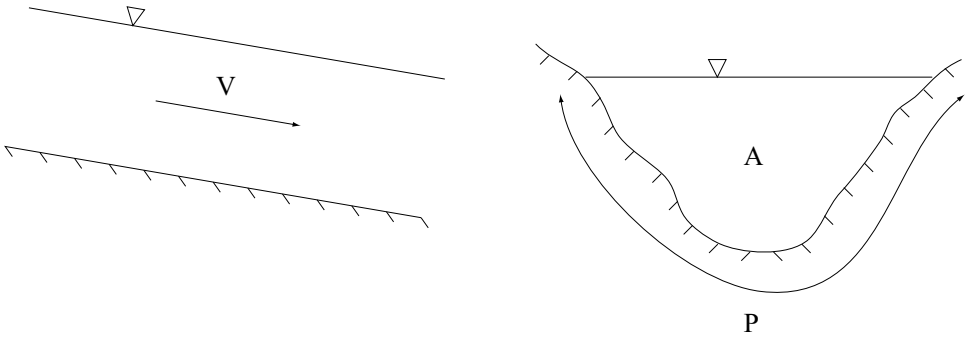

Figure 6.4: Sketch of elevation view and cross-sectional view of an open channel flow.

on the banks is $P' = FP$. Finally, by multiplying this reduced power by five months, one arrives at the amount of energy that is dissipated against the banks during the high-flow period of the year. Note that this will yield a conservative (i.e. high) estimate because, in reality, the distribution of dissipation is not expected to be uniform over the wetted perimeter, as has been assumed here. Rather, dissipation is expected to be higher in the middle of the stream, where the velocity is higher, and lower near the banks.

Site	S_f	P (W m^{-1})	F	P' (W m^{-1})	E (J m^{-1})
2 & 3	0.0003	215	0.0092	1.98	$2.6 \cdot 10^7$
4	0.0000051	0.0529	0.052	0.0028	$3.6 \cdot 10^4$
5	0.00026	36	0.025	0.89	$1.1 \cdot 10^7$

Table 6.9: Tabulated values of the dissipated energy, per meter of bank length, associated with the streamflow.

Comparing the figures from Tables 6.8 and 6.9, it is seen that the energy associated with boat wakes is roughly 2-5% that of the stream flow at Sites 2, 3, and 5. At Site 4, however, the relative contributions are reversed, with streamflow energy being roughly 4% that of the boat wake energy.

Recalling the earlier discussion of power vs. energy, note that, as shown in Table 6.9, the power on the banks ranges from ~ 1 W m^{-1} at Sites 2, 3, and 5 to ~ 0.001 W m^{-1} at Site 4. Regarding the average power associated with a wake train, it can be computed on a per-wave basis, from (3.1), and then averaged, or it can be estimated by dividing the energy in a wave train

by the duration of that wave train. Taking 30 s as a reasonable average wave train duration, estimates of boat wake power are summarized in Table 6.10

Boat	P (W m^{-1})
FG16	5
FG18	3
COM20	12
COM24	13
COM30	30
COM32	36

Table 6.10: Power, per unit meter of bank, of the wave trains of the different boats studied.

From these figures, it is seen that, even in the larger, more-energetic channels (Sites 2, 3, and 5), the *rate* of energy dissipation associated with the commercial boats considerably greater than that of the streamflow.

6.2.2 Shear Stress Calculations

Due to the no-slip boundary condition that exists between a flowing fluid and a solid surface, the velocity of the fluid at the surface itself is pinned to a value of zero and the velocity of the flow increases with distance from the surface (Fig. 6.5).

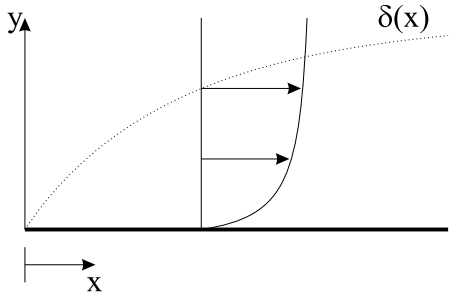

Figure 6.5: Sketch of a boundary layer over a solid surface.

As a result of this boundary layer structure, the fluid exerts shear on the surface. If the velocity profile is known and the flow is laminar, then the

shear stress at the surface is given by

$$\tau_0 = \mu \frac{dV}{dy}\bigg|_{y=0},$$

where μ is the absolute viscosity of the fluid ($1 \cdot 10^{-3}$ Pa s for water). If the flow, on the other hand, is turbulent, the same equation may be used, but a turbulent 'eddy' viscosity must be used in place of the absolute viscosity.

The boundary shear in an open channel flow can be deduced in another, indirect way. Considering a simple balance of forces in a reach characterized by uniform flow, the drag force provided by the boundary shear must balance the component of fluid weight along the slope of the bed. Put another way, the *average* boundary shear is given by

$$\tau_0 = \gamma R_h S_0.$$

Thus, at the study sites where sufficient data exist, we can calculate this average boundary shear. Next, it must be recognized that this shear is not uniform across the wetted perimeter of the channel. While the exact distribution is difficult to obtain, some guidance is provided by Lane (1955). Based upon studies of flow resistance in trapezoidal channels, that author suggests that the shear on the sides of the channel is roughly 75% of $\gamma R_h S_0$. Table 6.11 summarizes the estimated bank shear stresses for the study sites.

Site	τ_0 (Pa)
2 & 3	1.73
4	0.03
5	1.20

Table 6.11: Calculated bank shear stresses, due to streamflow.

The shear stress exerted by waves interacting with a boundary can also be calculated. Here, for the sake of simplicity, it will be assumed that the river bank is vertical and that water depth at the bank is h. As discussed in §3.2, waves impacting a vertical boundary result in a standing wave pattern. In this case, the amplitude of the periodic vertical velocity of the water at the bank is given by

$$w = \frac{H\omega}{2} \frac{\sinh[k(z+h)]}{\sinh(kh)},$$

where $z = 0$ corresponds to the water surface and $z = -h$ corresponds to the river bed.

At the free-surface, this velocity has a maximum value of $H\omega/2$. This periodic motion creates an oscillatory boundary layer at the bank itself. Details of the solution for the flow in this boundary layer can be found in Mei (1989) or White (1991). Assuming the boundary layer to be laminar, the maximum shear stress at the bank is given by

$$\tau_0 = \mu \frac{\sqrt{2}}{4} \omega H \sqrt{\frac{\omega}{\nu}}, \tag{6.3}$$

where ν is the kinematic viscosity of water, equal to $1 \cdot 10^{-6}$ m^2 s^{-1}.

As evidenced by the tables of results in Chapter 5, the average period of the boat wakes observed in this study is roughly 1 s, corresponding to an angular velocity of 6.28 rad s^{-1}. Thus, based upon the above formulation, waves with heights of 10 cm would exert a shear stress of approximately 0.55 Pa on the bank of the river, while waves with heights of 30 cm would exert a shear stress of approximately 1.65 Pa. These boat-associated shear stresses are therefore on the same order of magnitude as the streamflow shear stresses at Sites 2, 3, and 5. In the case of Site 4, which was the least-energetic site studied, the boat-associated shear stresses are two orders of magnitude greater than those due to the streamflow.

This analysis assumes that the boundary layers are laminar. According to Mei (1989), §8.7.1, oscillatory boundary layers become turbulent if

$$\frac{\omega U^2}{\nu} > 1.26 \cdot 10^4,$$

where U is the velocity amplitude just outside the boundary layer. For waves with periods similar to those in this study, this occurs when the wave height is only a few centimeters, suggesting that boat-wake boundary layers are generally turbulent.

In this case, the absolute viscosity in (6.3) should be replaced with an eddy viscosity, which is typically three orders of magnitude larger. The effect of this is that calculated boundary shear stresses will be roughly 30 times greater than the laminar predictions, suggesting that boat-wake shear stresses are considerably greater than streamflow shear stresses. This conclusion is corroborated by the OBS-3 measurements that show a significant spike in turbidity at the banks in response to a set of wakes.

Chapter 7

Conclusions & Recommendations

Near-bank boat-wake height and turbidity measurements were made at numerous sites on the Chilkat River during the summer of 2002. Several boats were studied, including those run by the Alaska Department of Fish & Game (ADFG) and those run by a commercial tour operator. To the extent possible, efforts were made to study the wake and turbidity characteristics under a wide range of conditions, including boat speed, passenger loading, water depth, and distance from shore.

A total of 68 trials were conducted and wave heights ranging from below the level of resolution of the instrumentation to above 30 cm were observed. In response to the loading of these waves on the banks of the river, suspended sediment concentration levels ranging from the ambient load of the river to in excess of 40 g l^{-1} were observed.

7.1 Conclusions

Some of the key findings of this report include:

- Turbidity measurements at the banks clearly demonstrate that boat wakes are capable of dislodging sediments from the banks. Peak values of suspended sediment concentration far outweigh the ambient load of the river and are found to increase with increasing wake height.

- Boat wakes are found to increase in amplitude with increasing boat size.

Measurements suggest that the wake train of the largest commercial boat studied contains roughly 10 times the energy of that of the smaller ADFG boat studied.

- While there is a well-known dependence upon boat speed (confirmed by the controlled measurements), boats navigating the upper Chilkat River tend to travel in a fairly narrow band of speed. This is largely due to the necessity of keeping the boats 'on-plane', or 'on-step'. Given the shallow water depths, these speeds ($15 - 25$ mph) correspond to high depth- and length-based Froude numbers. This is beneficial in minimizing wave heights at the banks.

- Boat wakes are found to decrease in amplitude with sailing line-to-bank distance. An equation is obtained which allows for the prediction of expected wave height at the bank as a function of boat size and sailing line distance. If a maximum allowable wave height at the bank is specified, this allows for the calculation of a minimum sailing line distance.

- Comparisons of streamflow and boat wake energy suggest that, in larger channels, boat wakes only make up 2-5% of the total energy dissipated annually against the banks. In smaller channels, the roles are reversed and the streamflow makes up only 2-5% of the annual energy dissipated.

- Comparisons of streamflow and boat wake *power* suggest that, in all channels, the *rate* of energy dissipation by boat wakes exceeds that of the streamflow.

- Comparisons of streamflow and boat wake shear stress at the banks suggest that the wakes are capable of exerting a larger shear stress than the streamflow.

In conclusion, it is the authors' belief that, despite the relatively low usage levels on the Chilkat River, the potential impacts associated with boating can not be ruled out. There is sufficient evidence for continued, longer-term monitoring of the situation.

7.2 Recommendations

Based upon the conclusions arrived at above, there are several specific recommendations that can be forwarded in an effort to minimize the impacts of boating on the banks and the bed of the Chilkat River.

- Using (6.1) and a specified maximum allowable wave height at the banks, a minimum suggested operating distance (between sailing line and shore) can be estimated. Using the observations of Nanson *et al.* (1994) that bank impact increases significantly beyond the threshold of $H_{max} \sim 30$ cm, these operating distances range from ~ 1 m for *FG16* to $\sim 10m$ for *COM32*. Using the more conservative observations of Dorova and Moore (1997) that bank impact increases significantly beyond the threshold of $H_{max} \sim 15$ cm, these operating distances range from ~ 5 m for *FG16* to ~ 60 m for *COM32*. That said, it is recognized that these distances will not always be possible to maintain, given (i) that many reaches are considerably narrower than this and (ii) that the main (i.e. deepest) path is often attached to one of the banks, preventing navigation down the middle of the channel.

- At any sailing distance less than that estimated in the previous recommendation, boat operators should avoid or minimize their time spent at certain speeds. This is based upon the well known behavior of boat wakes with depth- and length- based Froude numbers and the concept is illustrated in Fig. 7.1. Two speed 'bands' are shown, one developed from the depth-based criterion and the other developed from the length-based criterion.

  As an example, consider *COM32* ($L = 9.8$ m) operating in a water depth of $h = 1.5$ m. In order to avoid $Fr_d \sim 1$, it is clear that the boat should not operate in the range of 6.2 to 10.4 mph. In order to avoid $Fr_l \sim 0.5$, it is clear that the boat should not operate in the range of 8.1 to 13.8 mph. Thus, the entire range from 6.2 to 13.8 mph should be avoided, so as to minimize the impacts of this boat in this water depth.

- The banks of the Chilkat River are consistently characterized by a thick root mat overhanging a significant undercut. Relatively speaking, the erosive impacts of waves striking the root mat (where vegetation helps

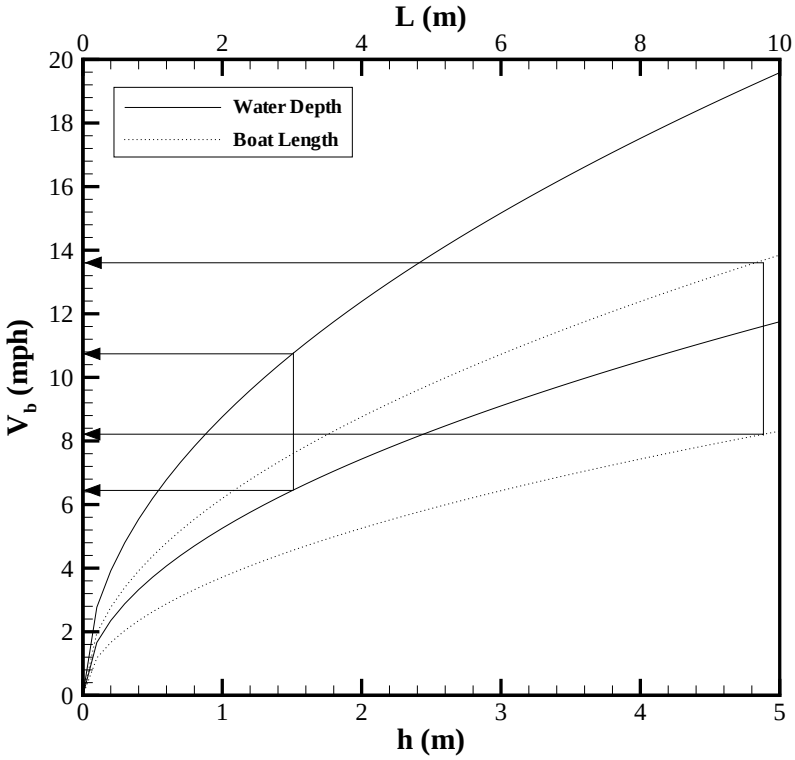

Figure 7.1: Speed bands to avoid, as functions of boat length and water depth, in order to minimize wakes.

to hold the bank together) compared to waves striking the undercut (where the soil is only loosely held together) will be less. As such, special consideration should be given to low-water periods where the water surface is in contact with the undercut.

7.3 Future Considerations

As discussed in Chapter 1, this pilot study was limited in scope. The main goals of documenting the hydraulic characteristics of the boats running the Chilkat River have largely been met. However, there are several issues and questions that would be suitable for attention in future studies.

- The number of trials that were performed in the initial study is rela-

tively low. An additional study period would give greater statistical significance to the results.

- Longer-term monitoring of bank erosion rates, both in active (boat traffic) and control (no boat traffic) channels would help quantify the increases in erosion associated with boating use. This can in part be accomplished by monitoring erosion pins, several dozen of which were installed during the 2002 field season.

- Only limited geotechnical assessment of bank composition was attempted. As erosion is strongly tied to bank characteristics, a more thorough survey of the banks and their stability is warranted.

- The third part of the 'problem', as conceptually broken down in §1.2 should be addressed. The banks and undercuts of the Chilkat are ideal rearing habitat for juvenile salmonids. The ambient hydraulic climate there is generally mild. The introduction to this climate of wake trains, and their associated increases in turbulence intensity, shear stress, and turbidity may be having some, as yet, unspecified level of impact on rearing fish populations.

  Therefore, additional study that more accurately quantifies levels of turbulence intensity, shear stress, dissipation, and so forth, along with potential laboratory studies on the correlation between these quantities and mortality levels, would provide valuable information to those responsible for managing the waters of the Chilkat River Basin.

Bibliography

ADNR, 2002. Chilkat bald eagle preserve management plan: public review draft. Technical report, Alaska Department of Natural Resources.

Arruda, J., G. Marzolf and R. Faulk, 1983. The role of suspended sediments in the nutrition of zooplankton in turbid reservoirs. Ecology, 64(5):1225–1235.

Beachler, M., 2002. The hydrodynamic impacts of recreational watercraft on shallow lakes. Master's thesis, The Pennsylvania State University.

Beachler, M. and D. Hill, 2002. Stirring up trouble? Resuspension of bottom sediments by recreational watercraft. Lake and Reservoir Management, in press.

Bhowmik, N., 1975. Boat-generated waves in lakes. Journal of the Hydraulic Division, 101:1465–1468.

Bhowmik, N., T. Soong, W. Reichelt and N. Seddik, 1992. Waves generated by recreational traffic on the Upper Mississippi River System. Technical Report EMTC 92-S003, Illinois State Water Survey, Champaign, IL.

Breitburg, D., 1988. Effects of turbidity on prey consumption by striped bass larvae. Transactions of the American Fisheries Society, 117:72–77.

Bugliosi, E., 1985. Hydrologic reconnaissance of the Chilkat River basin, southeast Alaska. Technical Report 84-618, United States Geological Survey.

Byrne, R., J. Boon, M.Alderson, C. Ostrom, C. Zabawa, T. Burnett, D. Blades, T. Deitz, M. Perry and R. Waller, 1980. Final report on the role of boat wakes in shore erosion in Anne Arundel County, Maryland. Coastal

Resources Division and Tidewater Administration, Marland Department of Natural Resources.

Derucher, K., G. Korfiatis and A. Ezeldin, 1994. Materials for Civil and Highway Engineers. Prentice-Hall, Inc., Englewood Cliffs, NJ 07632, 3rd edition.

Dorova, J. and G. Moore, 1997. Effects of boatwakes on streambank erosion, Kenai River, Alaska. Technical Report 97-4105, U.S. Geological Survey, Anchorage, Alaska, prepared in cooperation with the Alaska Department of Fish and Game.

Francisco, M., C. Ebbesmeyer, C. Boatman and T. Michelsen, 1999. Resuspension and transport of contaminated sediments along the Seattle waterfront, part 2: resuspension and transport mechanisms. J. Marine Env. Eng., 5:67–84.

Gucinski, H., 1982. Sediment suspension and resuspension from small-craft induced turbulence. U.S. EPA Chesapeake Bay Program, EPA 600/3-82-084.

Hamill, G., H. Johnston and D. Stewart, 1999. Propeller wash scour near quay walls. Journal of Waterway, Port, Coastal, and Ocean Engineering, 125(4):170–175.

Herbich, J., 1984. Sediment movement induced by ship propellers. Marcel Dekker, Inc., New York.

Johnson, P., G. Gleason and R. Hey, 1999. Rapid assessment of channel stability in vicinity of road crossing. Journal of Hydraulic Engineering, 125(6):645–651.

Johnson, S., 1994. Recreational boating impact investigations - Upper Mississippi River System, Pool 4, Redwing, Minnesota. Technical Report EMTC 94-S004, Minnesota Department of Natural Resources.

Killgore, K., A. Miller and K. Conley, 1987. Effects of turbulence on yolk-sac larvae of paddlefish. Transactions of the American Fisheries Society, 116:670–673.

Kirkegaard, J., H. Kofoed-Hansen and B. Elfrink, 1998. Wake wash of high-speed craft in coastal waters. In Proceedings of the 26th Coastal Engineering Conference, pages 325–337, ASCE, Copenhagen, Denmark.

Lamb, H., 1932. Hydrodynamics. Dover, Sixth edition.

Lane, E., 1955. Design of stable channels. Transactions of the American Society of Civil Engineers, 120:1234–1260.

Liddle, M. and H. Scorgie, 1980. The effects of recreation on freshwater plants and animals: a review. Biological Conservation, 17:183–206.

Maynord, S., 1998. Bottom shear stress from propeller jets. In Proceedings of the Ports '98 Conference, pages 1074–1083, ASCE, Long Beach, CA, USA.

Maynord, S., 2001. Boat waves on Johnson Lake and Kenai River, Alaska. Technical Report ERDC/CHL TR-01-31, U.S. Army Corps of Engineers, prepared for the Alaska Department of Fish and Game.

MCA, 2001. A physical study of fast ferry wash characteristics in shallow water. Technical Report Research Project 457, The Maritime and Coastguard Agency.

Mei, C., 1989. The applied dynamics of ocean surface waves, volume 1 of *Advanced Series on Ocean Engineering*. World Scientific.

Morgan, R., R. Ulanowicz, V. R. Jr. L. Noe and G. Gray, 1976. Effects of shear on eggs and larvae of striped bass, *Morone Saxatilis*, and white perch, *M. Americana*. Transactions of the American Fisheries Society, 106:149–154.

Nanson, G., A. Von-Krusenstierna, E. Bryant and M. Renilson, 1994. Experimental measurements of river-bank erosion caused by boat-generated waves on the Gordon River, Tasmania. Regulated Rivers: Research and Management, 9(1):1–14.

Nielson, P., 1992. Coastal bottom boundary layers and sediment transport, volume 4 of *Advanced Series on Ocean Engineering*. World Scientific.

Parchure, T., W. M. Jr. and A. Teeter, 2001. Desktop method for estimating vessel-induced sediment suspension. Journal of Hydraulic Engineering, 127(7):577–587.

Parnell, K. and H. Kofoed-Hansen, 2001. Wakes from large high-speed ferries in confined coastal waters: management approaches with examples from New Zealand and Denmark. Coastal Management, 29:217–237.

Sorenson, R., 1973a. Ship-generated waves. In V. Chow, editor, Advances in Hydroscience, volume 9, pages 49–83, Academic Press.

Sorenson, R., 1973b. Water waves produced by ships. Journal of the Waterways Harbors and Coastal Engineering Division, 99(2):245–256.

Stumbo, S., K. Fox, F. Dvorak and L. Elliot, 1999. The prediction, movement adn analysis of wake wash from marine vessels. Marine Technology, 36(4):248–260.

Sturm, T., 2001. Open channel hydraulics. McGraw Hill.

Sutherland, A. and D. Ogle, 1975. Effect of jet boats on salmon eggs. New Zealand Journal of Marine and Freshwater Research, 9(3):273–282.

Wagner, K., 1991. Assessing impacts of motorized watercraft on lakes: issues and perceptions. In Proceedings of a National Conference on Enhancing States' Lake Management Programs, pages 77–93, Northeastern Illinois Planning Commission.

White, F., 1991. Viscous fluid flow. McGraw-Hill, 2nd edition.

WHOI, 1998. The environmental impacts of boating. Technical Report WHOI-98-03, Woods Hole Oceanographic Institution, Woods Hole, MA, proceedings of a workshop held December 7-9, 1994.

Yousef, Y., W. McLellon, R. Fagan, H. Zebuth and C. Larrabee, 1978. Mixing effects due to boating activities in shallow lakes. Technical Report ESEI N. 78-10, Florida Technological University.

Yousef, Y., W. McLellon and H. Zebuth, 1980. Changes in phosphorous concentrations due to mixing by motorboats in shallow lakes. Water Research, 14:841–852.